Extension of scaled particle theory to inhomogeneous hard particle fluids. IV. Cavity growth at any distance relative to a planar hard wall

Daniel W. Siderius and David S. Corti

Extension of scaled particle theory to inhomogeneous hard particle fluids. IV. Cavity growth at any distance relative to a planar hard wall

Daniel W. Siderius[*] and David S. Corti

School of Chemical Engineering, Purdue University, and

480 Stadium Mall Drive, West Lafayette, IN 47907-2100, USA

Abstract

A completely generalized version of an inhomogeneous scaled particle theory (I-SPT) for hard particle fluids confined by hard walls is presented, whereby the reversible work of cavity insertion can be determined for a cavity of any radius located at any distance from the hard wall. New exact and approximate conditions on the central function $\overline{G}$ of I-SPT are developed, where $\overline{G}$ is related to the average value of the anisotropic density of hard-sphere centers at the surface of the cavity. The predictions of the work of insertion and the form of $\overline{G}$ are quite accurate up to moderate bulk densities as compared to molecular simulation results. The accuracy of I-SPT begins to decline at high densities, due to limitations of certain needed approximations required for a complete description of $\overline{G}$. Finally, interesting insights into the origin of depletion effects between a hard-sphere solute and the hard wall are generated via this version of I-SPT. The oscillatory nature of depletion forces, exhibiting both attractive and repulsive domains, is found to arise from the interplay between bulk SPT and I-SPT relations.

[*]Present Address: National Institute of Standards and Technology, 100 Bureau Drive, Gaithersburg, MD 20899, USA

I. INTRODUCTION

In light of the success of scaled particle theory (SPT), originally introduced in 1959[1], in describing the behavior of both hard particle and soft-core fluids[2–19], an initial extension of SPT to inhomogeneous hard particle fluids was recently developed[20, 21]. Labeled as I-SPT, the nonuniform fluid density that develops near a hard, structureless wall was explicitly taken into account during the derivation of standard SPT relations. As a result, new physical and geometric insights were generated into the structural changes brought about by the insertion of cavities near a wall. While accurately predicting the reversible works of cavity insertion, this version of I-SPT was limited to those cases for which the cavity exposed to the nonuniform fluid adjacent to the wall has a volume equal to or less than that of a hemisphere. In addition, only cavities that were "grown" radially about a fixed center coordinate were considered.

A subsequent paper[22] showed how cavities beyond the hemisphere, though still intersecting the wall, could be included into I-SPT. Rather than growing a cavity radially at a fixed location, this version of I-SPT considered instead the (effective) forces needed to "push" a cavity into the fluid when starting from a position behind the wall. Such a route was chosen since it allowed for additional conditions to be incorporated into I-SPT, as well as avoiding some (at the time) unresolved issues that arise if one were to consider the radial growth of cavities beyond the wall. This version of I-SPT also provided useful information about the physical and geometric origins of depletion interactions in hard particle systems [23–28]. Given that the cavities were required to intersect the wall, depletion interactions could only be generated over a small range of the full depletion potential.

Despite their successes, neither of the two above-mentioned forms of I-SPT reach the desired for goal that provided the initial intent for extending SPT to inhomogeneous systems: describing the radial growth of cavities that are centered at any coordinate relative to the hard wall. Since their introduction, however, the understanding of the boundary thermodynamics of cavities intersecting a wall has improved[29]. As such, previously missing information has now become available for the development of a sufficiently accurate and fully generalized form of I-SPT. And so, we present in this paper a version of I-SPT that yields expressions (some exact, others approximate) for the reversible work of inserting a cavity of any radius located at any distance from a hard wall. We identify a number of new

I-SPT conditions, based again on physical and geometric arguments, each of which provides additional insights into the behavior of hard particle fluids near planar surfaces, as well as improving the accuracy of some earlier versions of I-SPT.

While the further development of I-SPT is important in itself, our aim is not simply to extend the range of applicability of I-SPT. For one, as discussed in Ref. [29], a form of I-SPT that can describe cavities that are grown radially at any location is necessary for an accurate determination of the line tension of cavities that intersect a planar surface. A generalized version of I-SPT will provide the required inputs, such as the work of cavity formation, needed to estimate this important thermodynamic property.

Furthermore, due to the equivalence of cavities and hard-sphere solutes, I-SPT relations can be used to predict the depletion, or entropic, force between a hard sphere solute and a hard wall. The development of accurate expressions for entropic forces are of interest, given that entropic interactions are important in governing the behavior of hard-sphere-like fluids and can be utilized to control the self-assembly of model colloidal dispersions [30–36]. SPT was previously employed to estimate the depletion force between a hard colloid and a hard wall[37], though the use of bulk relations led to inaccurate predictions at high fluid densities. I-SPT, with its explicit incorporation of the nonuniformity of the hard sphere fluid near the hard wall, is well suited to studying depletion interactions. One of the earlier versions of I-SPT[22] yielded predictions of the depletion force exerted on a large diameter hard-sphere colloid near a wall that were in excellent agreement with molecular simulation results. As noted earlier, the range of the depletion force that was described by this version of I-SPT was limited, which the current extension presented here overcomes. Hence, I-SPT can now generate predictions of the depletion force for all separations and for all hard sphere solute diameters. Here, we use I-SPT to provide insight into the origin and oscillatory nature of depletion forces. In particular, both attractive and repulsive depletion forces are easily explained using bulk SPT and I-SPT relations, which manifest the different behaviors exhibited by cavities within SPT and I-SPT.

The paper is organized as follows. In Section 2, a review of bulk SPT and all the current versions of I-SPT is provided. In Section 3, the further extension of I-SPT is presented. Here, the new conditions required to describe the radial growth of cavities at all distances from the hard, structureless wall are introduced. In addition, the interpolations needed to describe the average contact density around the cavity, beyond the ranges at which this

quantity is known exactly, are presented. The comparison between the predictions of I-SPT and the results of molecular simulation are included in Section 4. A discussion of depletion effects and how they can be determined from I-SPT is provided in Section 5. Conclusions are presented in Section 6.

II.   REVIEW OF SPT AND EXTANT I-SPT

Before introducing the updated version of I-SPT, we first present a review of both SPT for the homogeneous hard-sphere (HS) fluid and the various existing versions of I-SPT (more detailed discussions of SPT and I-SPT can be found in Refs. [1, 38–41] and Refs. [20–22], respectively). The starting point of any version of SPT is the introduction of a cavity of radius λ into a solvent of HS of diameter σ, where the cavity is defined as a spherical region devoid of HS centers. A cavity in a HS fluid can also be considered as a HS solute of radius σ_s, where $\lambda = (\sigma_s + \sigma)/2$[1] (albeit with the possibility of negative diameters, in which $\lambda \geq 0$ implies $\sigma_s \geq -\sigma/2$). Accordingly, the cavity becomes equivalent to a solvent HS when $\lambda = \sigma$.

For uniform, unconfined fluids, all thermophysical properties are related to the central SPT function $G(\lambda)$, where $\rho G(\lambda)$ is defined as the local density of HS centers at the surface of a cavity of radius λ and ρ is the number density of HS centers far from the cavity. Since $\rho G(\lambda) kT$ is the local stress normal to the cavity surface (in which k is Boltzmann's constant and T is the absolute temperature), the reversible work, $W(\lambda)$, of growing or adding a cavity of radius of at least λ within the fluid is related to G via the following integral[1]

$$W(\lambda) = 4\pi\rho kT \int_0^\lambda G(r) r^2 dr. \tag{1}$$

G is known exactly for $\lambda \leq \sigma/2$, after which it is represented by one or more interpolation functions that are constrained by several exact conditions[1, 39–42]. Typically, the interpolation(s) takes the form of a Laurent series[1, 43]

$$G(\lambda) = \alpha_0(\rho) + \frac{\alpha_1(\rho)}{\lambda} + \frac{\alpha_2(\rho)}{\lambda^2} + \frac{\alpha_4(\rho)}{\lambda^4} + \cdots \tag{2}$$

in which several of the fitting parameters, $\alpha_i(\rho)$, are related to particular thermophysical properties of the HS fluid. For example, in the final (or only, if a single interpolation function is invoked) Laurent series, one notes that $\alpha_0(\rho) = G(\infty) = p/\rho kT$, where p is

4

the pressure of the HS fluid, while $\alpha_1 (\rho) = \gamma_\infty \sigma^2 / 2kT$, where γ_∞ is the surface (or, more properly, boundary) tension of a planar surface in contact with a HS fluid. Once $G(\lambda)$ is known, numerous other properties of the HS fluid may be obtained from the chosen set of interpolations for $G(\lambda)$.

Inhomogeneous SPT is the application of SPT ideas to a HS fluid confined by planar walls. I-SPT, however, must acknowledge the following two major departures from SPT: 1) a cavity may intersect a wall and 2) the properties of the fluid near the wall are not uniform. Due to the loss of radial symmetry about a cavity in a nonuniform fluid, one is required to introduce a modified version of $G(\lambda)$ that includes information about the cavity's location relative to a wall. Thus, the central I-SPT function is $G(\lambda, \theta, h)$, where $\rho G(\lambda, \theta, h)$ is the local density of HS centers at a position identified by λ, θ, and h[20] (and is yet again related to the local stress normal to the cavity surface at that same position). As shown in Fig. 1(a), h locates the position of the cavity relative to the effective wall (or the $z = 0$ plane, indicating the closest approach of HS centers to the wall) and θ is the azimuthal angle that identifies a particular position on the cavity surface. The introduction of an average of $G(\lambda, \theta, h)$ over θ, denoted by $\overline{G}(\lambda, h)$, proved useful for further manipulations. For example, for cavities in which $h \leq 0$, the work of adding a cavity to the system is given by[20]

$$W(\lambda, h) = 2\pi \rho kT \int_0^\lambda \overline{G}(r, h) \left(r^2 + rh \right) dr. \tag{3}$$

Furthermore, $\overline{G}$ for $h \leq 0$ and $\lambda \leq \sqrt{h^2 + (\sigma/2)^2}$ is known exactly and is equal to[20]

$$\rho \overline{G}(\lambda, h) = \frac{\int_0^{\lambda+h} \rho(z) \, dz}{(\lambda + h) \left(1 - \pi \int_0^{\lambda+h} \rho(z) \left[\lambda^2 - (z - h)^2 \right] dz \right)} \qquad \lambda \leq \sqrt{h^2 + \left(\frac{\sigma}{2} \right)^2}, \tag{4}$$

where $\rho(z)$ is the local density of HS centers at a position z relative to the wall (see Fig. 1). [Note that I-SPT requires some form of $\rho(z)$ as input, and cannot in its present development be used to generate $\rho(z)$ independently.] Beyond this range of cavity radii, a Laurent series interpolation of the following form was proposed as an approximation of $\overline{G}$[20]

$$\overline{G}(\lambda, h) = \beta_0(\rho, h) + \frac{\beta_1(\rho, h)}{\lambda + h} + \frac{\beta_2(\rho, h)}{\lambda(\lambda + h)} + \frac{\beta_4(\rho, h)}{\lambda^3(\lambda + h)} \qquad \lambda > \sqrt{h^2 + \left(\frac{\sigma}{2} \right)^2}, \tag{5}$$

where the fitting coefficients $\beta_i(\rho, h)$ were obtained via additional exact conditions on $\overline{G}$. These exact conditions include the continuity of $\overline{G}$ and its first derivative with respect to λ at $\lambda = \sqrt{h^2 + (\sigma/2)^2}$, the asymptotic limit of $\overline{G}(\infty) = p/\rho kT$ and a condition related to

the excess chemical potential, μ^{ex}, of the HS fluid. Unlike bulk SPT, which can be used to generate a prediction of p and μ^{ex}, I-SPT requires that these quantities be provided from an outside source, such as the Carnahan-Starling equation of state[44]. A modified interpolation and a new condition relating β_1 to γ_∞ (the value of which is again provided by an equation of state) not included in the original formulations of I-SPT were introduced in Ref. [22].

To extend the ideas of I-SPT to cavities located at $h > 0$, a different version of I-SPT was derived, in which the cavity is "pushed" into the fluid from behind the wall while holding λ fixed[22] rather than "growing" the cavity from a static center point. A different type of average I-SPT function was necessary and was denoted by $\overline{F}(\lambda, h)$, though it is still related to an integral of $G(\lambda, \theta, h)$. $\overline{F}$ is proportional to the force perpendicular to the wall exerted by the fluid on the cavity and, like $\overline{G}$, is known exactly for certain configurations and must be interpolated thereafter. Here, the work of adding a cavity to the fluid is given by[22]

$$W(\lambda, h) = 2\pi \rho k T \int_{-\lambda}^{h} \overline{F}(\lambda, z)\, dz. \tag{6}$$

For the cases previously considered, such that the cavity always intersected the wall or $h \leq \lambda$, $\overline{F}$ is exactly known for $h \leq -\sqrt{\lambda^2 - \left(\frac{\sigma}{2}\right)^2}$[22]

$$\overline{F}(\lambda, h) = \frac{\int_0^{h+\lambda} \rho(z)(z-h)\, dz}{\rho \lambda^2 \left(1 - \pi \int_0^{h+\lambda} \rho(z)\left[\lambda^2 - (z-h)^2\right] dz\right)} \quad h \leq -\sqrt{\lambda^2 - \left(\frac{\sigma}{2}\right)^2}. \tag{7}$$

Beyond this exact limit, $\overline{F}$ was interpolated not using a Laurent series but with a set of polynomials that satisfactorily mimicked the true behavior of $\overline{F}$. The fitting coefficients were again obtained by invoking various exact conditions on $\overline{F}$, such as the continuity of $\overline{F}$ and its first derivative with respect to h at $h = -\sqrt{\lambda^2 - (\sigma/2)^2}$ as well as formal limits of macroscopic thermodynamics[22]. Other approximate, though reasonably accurate, conditions were generated in order to better match the behavior of $\overline{F}$ at intermediate values of h. The interpolation procedure for $\overline{F}$ is much more complex than that for $\overline{G}$, though nonetheless proved to be highly accurate up to moderate fluid densities and, perhaps more importantly, uncovered new phenomena in the physics of depletion forces in HS colloidal dispersions[22].

While successful, these previous versions of I-SPT were, however, limited in application to those cavities that intersect the effective wall. As such, they provided no description of

6

$\overline{G}(\lambda, h)$ for $h > 0$. Additionally, the previous versions of I-SPT provided no firm theoretical justification for the chosen interpolation series. The interpolation series were based partly on expectations of macroscopic thermodynamic results and partly on intuition. Taken together, these two issues provide the motivation for revisiting I-SPT and extending this previous framework to the description of cavities for which $h > 0$ and $\lambda < h$.

III. I-SPT: RADIAL GROWTH OF CAVITIES CENTERED AT $h > 0$

The earlier versions of I-SPT were successful in their stated aim of computing the work of inserting cavities that intersect a planar surface. We are now, however, interested in describing any cavity that is located near a planar surface, specifically those locations that satisfy $h \geq 0$ without also requiring $\lambda > h$ (i.e., no overlap of the $z = 0$ plane). For various reasons, we choose to extend the $\overline{G}$ description of cavities to $h > 0$. Hence, the derivation of the new extension of I-SPT will proceed via the I-SPT derivation presented in Ref. [20].

In our examination of cavities centered at $h > 0$, we again utilize the coordinate system identified in Fig. 1(a). Furthermore, as illustrated in Fig. 1(b), the accessible values of θ for $\lambda < h$ now span from 0 to π, rather than 0 to $\cos^{-1}(-h/\lambda)$ as is the case for $\lambda > h$. Finally, we again define an I-SPT function $G(\lambda, \theta, h)$ such that $\rho G(\lambda, \theta, h)$ is the local density on the cavity surface at an angle θ, with $\rho G(\lambda, \theta, h) kT$ providing the local stress normal to the cavity surface at θ.

A. I-SPT Functions and Definitions

Using arguments identical to those invoked to obtain $\overline{G}(\lambda, h)$ for $h \leq 0$ in Ref. [20], the reversible work required to differentially increase the radius of a cavity centered at h may be written as

$$dW = \left(\int_{A(\lambda, h)} \rho G(\lambda, \theta, h) kT dA \right) d\lambda, \tag{8}$$

where $A(\lambda, h)$ is the surface area of the cavity accessible to the fluid of hard-spheres (i.e., that portion of the cavity residing at $z \geq 0$ in Fig. 1). The above equation, in essence, states that the differential work of growing the cavity is the total normal force on the cavity surface multiplied by the differential change in radius. Equation 8 is valid for any value of h and, through subtle manipulation, could be transformed to describe the work of growing a cavity

7

near any confining surface. (Chapter 4 of Ref. [45] includes a discussion of an entirely general I-SPT based on this idea.) As was done previously, though not explicitly noted, $A(\lambda, h)$ is easily transformed to an integral over θ and some terms related to λ. Unlike the previous derivation for $h \leq 0$, $A(\lambda, h)$ cannot, however, be represented by a single function. Due to the abrupt change in the bounds of θ at $\lambda = h$ (where the cavity just touches the $z = 0$ plane) we are required to write one expression valid for $\lambda \leq h$ and another for $\lambda > h$. $\partial W / \partial \lambda$ must therefore be expressed as

$$\frac{\partial W}{\partial \lambda} = \begin{cases} 2\pi \lambda^2 \int_0^\pi G(\lambda, \theta, h) \sin \theta d\theta & \lambda \leq h \\ 2\pi \lambda^2 \int_0^{\cos^{-1}\left(\frac{-h}{\lambda}\right)} G(\lambda, \theta, h) \sin \theta d\theta & \lambda > h \end{cases}. \tag{9}$$

Following Ref. [20], we now replace the integrals of $G(\lambda, \theta, h)$ by some other function, since $G(\lambda, \theta, h)$ cannot be recovered directly from W. Just as $\overline{G}(\lambda, h)$ for $h \leq 0$ was defined as an average of $G(\lambda, \theta, h)$ over the surface of the cavity, we likewise define a similar function for $h > 0$. Again due to the abrupt change in $A(\lambda, h)$ at $\lambda = h$, the relevant definitions of $\overline{G}(\lambda, h)$ for $h > 0$ are given by

$$\overline{G}(\lambda, h) = \begin{cases} \dfrac{2\pi \lambda^2 \int_0^\pi G(\lambda, \theta, h) \sin \theta d\theta}{2\pi \lambda^2 \int_0^\pi \sin \theta d\theta} & \lambda \leq h \\ \dfrac{2\pi \lambda^2 \int_0^{\cos^{-1}\left(\frac{-h}{\lambda}\right)} G(\lambda, \theta, h) \sin \theta d\theta}{2\pi \lambda^2 \int_0^{\cos^{-1}\left(\frac{-h}{\lambda}\right)} \sin \theta d\theta} & \lambda > h \end{cases}$$

$$= \begin{cases} \dfrac{1}{2} \int_0^\pi G(\lambda, \theta, h) \sin \theta d\theta & \lambda \leq h \\ \dfrac{\lambda}{\lambda + h} \int_0^{\cos^{-1}\left(\frac{-h}{\lambda}\right)} G(\lambda, \theta, h) \sin \theta d\theta & \lambda > h \end{cases} \tag{10}$$

in which we note that

$$A(\lambda, h) = \begin{cases} 4\pi \lambda^2 & \lambda \leq h \\ 2\pi (\lambda^2 + \lambda h) & \lambda > h \end{cases} \tag{11}$$

Substitution of Eq. 10 into Eq. 9, followed by integration from $\lambda = 0$ to a final radius of λ allows the reversible work of growing a cavity of radius λ centered at h to be written as

$$W(\lambda, h) = \begin{cases} 4\pi \rho kT \int_0^\lambda \overline{G}(r, h) r^2 dr & \lambda \leq h \\ W(h, h) + 2\pi \rho kT \int_h^\lambda \overline{G}(r, h) (r^2 + rh) dr & \lambda > h \end{cases}, \tag{12}$$

where, for convenience, $W(h, h)$ represents an integral from the first line of the above equation. While $W(h, h)$, the work of inserting a cavity of radius h that is located a distance h from the effective wall, is identically zero for $h \leq 0$ (where here $\lambda = |h|$), $W(h, h) \neq 0$ for

8

$h > 0$. The definition of $\overline{G}$ for $\lambda > h$ is identical to that for $h \leq 0$ and all values of λ[20]. We repeatedly find that expressions related to W or $\overline{G}$ for $\lambda > h > 0$ are common to all values of h, a property that derives from $A(\lambda, h)$ being described by a similar function provided that $\lambda > h$ (which is automatically satisfied when $h \leq 0$).

For $\lambda = h$, we note that the two expressions for $\overline{G}$ both yield

$$\overline{G}(h, h) = \frac{1}{2} \int_0^\pi G(h, \theta, h) \sin \theta d\theta. \tag{13}$$

Given that G is proportional to the normal stress at the surface of the cavity, which in turn is related to the density distribution of HS centers around the cavity, there is no reason to expect that $G(h, \theta, h)$ changes discontinuously as $\lambda \to h$ from above and below. Thus, Eq. 13 indicates that $\overline{G}(h, h)$ is continuous at $\lambda = h$. (As we discuss later, the continuity of $\overline{G}$ at $\lambda = h$ may be confirmed exactly for $h \leq \sigma/2$ while simulation results for larger h support this conclusion.)

Continuity does not extend, however, to the first derivative of $\overline{G}$ with respect to λ evaluated at $\lambda = h$. For $\lambda < h$, we find that

$$\frac{\partial \overline{G}}{\partial \lambda} = \frac{1}{2} \int_0^\pi \frac{\partial G(\lambda, \theta, h)}{\partial \lambda} \sin \theta d\theta \qquad \lambda \leq h, \tag{14}$$

while for $\lambda > h$, we have that

$$\frac{\partial \overline{G}}{\partial \lambda} = \frac{\lambda}{\lambda + h} \int_0^{\cos^{-1}\left(\frac{-h}{\lambda}\right)} \frac{\partial G(\lambda, \theta, h)}{\partial \lambda} \sin \theta d\theta$$
$$+ \frac{h}{(\lambda + h)^2} \int_0^{\cos^{-1}\left(\frac{-h}{\lambda}\right)} G(\lambda, \theta, h) \sin \theta d\theta - \frac{h}{\lambda^2 + \lambda h} G\left(\lambda, \cos^{-1}(-h/\lambda), h\right) \qquad \lambda > h. \tag{15}$$

Evaluating both derivatives at $\lambda = h$ and taking the difference, we obtain

$$\Delta \left[\frac{\partial \overline{G}}{\partial \lambda}\right]_{\lambda = h} \equiv \left.\frac{\partial \overline{G}}{\partial \lambda}\right|_{\lambda = h^+} - \left.\frac{\partial \overline{G}}{\partial \lambda}\right|_{\lambda = h^-}$$
$$= \frac{1}{2} \int_0^\pi \left(\left.\frac{\partial G(\lambda, \theta, h)}{\partial \lambda}\right|_{\lambda = h^+} - \left.\frac{\partial G(\lambda, \theta, h)}{\partial \lambda}\right|_{\lambda = h^-}\right) \sin \theta d\theta$$
$$+ \frac{1}{2h} \left[\overline{G}(h, h) - G(h, \pi, h)\right], \tag{16}$$

where the superscripts '-' and '+' indicate that the given term is evaluated infinitesimally below or above $\lambda = h$, respectively. The above result suggests that $\partial \overline{G}/\partial \lambda$ is in general discontinuous at $\lambda = h$, since previous work indicates that $\overline{G}(h, h) \leq G(h, \pi, h)$. For the

9

cavity just touching the $z = 0$ plane, a large density enhancement of HS centers occurs within the cusp region $(\theta \to \pi)$, in which $G(h, \pi, h) \geq p/\rho kT$[21], while $\overline{G}(\lambda, h) \leq p/\rho kT$[20], implying that the third line of Eq. 16 is always negative. Nevertheless, the sign of the discontinuity of $\partial \overline{G}/\partial \lambda$ is not entirely clear, since the integral portions of Eq. 16 may not cancel identically. Although $G(\lambda, \theta, h)$ is continuous at $\lambda = h$, the manner in which the local density along the cavity surface varies with λ may be different (particularly for $\theta \to \pi$) when the cavity is already intersecting the wall and its radius decreases to the limit where it just touches the wall as compared to when the cavity begins by not intersecting the wall and its radius increases to the limit where it again just touches the wall. In the former case, HS centers can only reach $\theta = \pi$ when $\lambda \to h$; in the latter case, HS centers always have access to $\theta = \pi$ except when $\lambda \to h$[25–27, 46, 47].

Exact expressions for $\overline{G}$ provided below do reveal that the integral term in Eq. 16 does vanish for $\lambda \leq \sigma/2$ (though the remaining term is not zero). Yet, the approximations invoked to describe $\overline{G}$ at larger λ, as well as a boundary thermodynamic analysis for macroscopic cavities, suggest that the integral term is not zero in general. (Due to sampling problems inherent in the determination of $G(\lambda, \theta, h)$, and particularly its derivative with respect to λ, molecular simulations results were unfortunately inconclusive about the sign of this integral term.)

B. Exact I-SPT Expressions

Similar to previous versions of SPT and I-SPT, we now relate $\overline{G}(\lambda, h)$ to the probability of observing a cavity of radius of at least λ centered at $z = h$, $P_0(\lambda, h)$, and then make use of exact knowledge of P_0 to identify $\overline{G}$ exactly under certain conditions. Given that $P_0 = \exp(-W/kT)$, Eqs. 9 and 10 indicate

$$\rho \overline{G}(\lambda, h) = \begin{cases} \dfrac{-1}{4\pi\lambda^2} \dfrac{\partial \ln P_0(\lambda, h)}{\partial \lambda} & \lambda \leq h \\ \dfrac{-1}{2\pi(\lambda^2 + \lambda h)} \dfrac{\partial \ln P_0(\lambda, h)}{\partial \lambda} & \lambda > h \end{cases} \tag{17}$$

The relation for $\overline{G}$ in terms of P_0 for $\lambda > h$ is again identical to that for $h \leq 0$[20].

Now, P_0 may be interpreted in the following manner[1, 22]. Suppose that spheres of radius λ are drawn concentric with all solvent hard-spheres in a particular configuration. Then, for that configuration, the probability of locating a cavity of radius of at least λ

centered at $z = h$ is the area fraction of the $z = h$ plane not eclipsed by the spheres of radius λ. P_0 is then obtained by ensemble averaging over all possible configurations. With this interpretation, P_0 is given by[22]

$$P_0\left(\lambda, h\right) = 1 + \sum_{m=1}^{\infty}\left(-1\right)^m F_m\left(\lambda, h\right), \qquad (18)$$

where $F_m\left(\lambda, h\right)$ is the average area fraction of the $z = h$ plane eclipsed by the mutual intersection of m spheres of radius λ. Depending on the value of λ, not all F_m terms are required[22]. For example, when $\lambda \leq \sigma/2$ and $h > 0$, two spheres of radius λ concentric with solvent HS (of diameter σ) cannot intersect on the $z = h$ plane. Hence, only F_1 is needed. Similarly, two spheres of radius λ may intersect for $\sigma/2 < \lambda \leq \sigma/\sqrt{3}$, but three may not, requiring that $F_m\left(\lambda, h\right) = 0$ for $m \geq 3$ in this subdomain, and so on. Computation of F_m is then accomplished by identifying the various radial subdomains and representing the necessary F_m terms by nontrivial integrals that count successive overlapping circles that eclipse the $z = h$ plane. Following Refs. [20–22], F_1 may be expressed as

$$F_1\left(\lambda, h\right) = \begin{cases} \pi \int_{h-\lambda}^{h+\lambda} \rho\left(z\right)\left[\lambda^2 - \left(z - h\right)^2\right] dz & \lambda \leq h \\ \pi \int_{0}^{h+\lambda} \rho\left(z\right)\left[\lambda^2 - \left(z - h\right)^2\right] dz & \lambda > h \end{cases}, \qquad (19)$$

Referring to Appendix A of Ref. [22], F_2 may be written as

$$F_2\left(\lambda, h\right) = \begin{cases} \pi \int_{h-\lambda}^{h+\lambda} dz_1 \int_{h-\lambda}^{h+\lambda} dz_2 \int_{0}^{r_{\max}} \rho^{[2]}\left(z_1, z_2, r\right) \Omega_2\left(z_1, z_2, r, \lambda, h\right) r\, dr & \lambda \leq h \\ \pi \int_{0}^{h+\lambda} dz_1 \int_{0}^{h+\lambda} dz_2 \int_{0}^{r_{\max}} \rho^{[2]}\left(z_1, z_2, r\right) \Omega_2\left(z_1, z_2, r, \lambda, h\right) r\, dr & \lambda > h \end{cases}, \qquad (20)$$

where $\rho^{(2)}\left(z_1, z_2, r\right)$ is the pair distribution function for two hard-spheres located at z_1 and z_2 with an in-plane distance (parallel to the wall) r between them and $\Omega_2\left(z_1, z_2, r, \lambda, h\right)$ is the area on the $z = h$ plane eclipsed by the mutual overlap of the circles projected by spheres of radius λ concentric with the same two hard-spheres. The value of r for which Ω_2 vanishes for a given z_1 and z_2 is $r_{max} = \sqrt{\lambda^2 - \left(z_1 - h\right)^2} + \sqrt{\lambda^2 - \left(z_2 - h\right)^2}$. As shown in Ref. [22], Ω_2 yields a divergent third derivative of F_2 with respect to λ as $\lambda \to \sigma/2^+$, which implies that $\partial^2 \overline{G}/\partial \lambda^2 \to -\infty$ as $\lambda \to \sigma/2^+$ for $h > 0$.

As stated previously, only F_1 is required for $\lambda \leq \sigma/2$. Entering $P_0 = 1 - F_1$ into Eq. 17

yields the following exact expression for $\overline{G}$

$$\rho\overline{G}\left(\lambda,h\right)=\begin{cases}\dfrac{\int_{h-\lambda}^{h+\lambda}\rho(z)dz}{2\lambda\left(1-\pi\int_{h-\lambda}^{h+\lambda}\rho(z)\left[\lambda^2-(z-h)^2\right]dz\right)} & \lambda\leq\frac{\sigma}{2} \\ & \lambda\leq h \\ \dfrac{\int_0^{h+\lambda}\rho(z)dz}{(\lambda+h)\left(1-\pi\int_0^{h+\lambda}\rho(z)\left[\lambda^2-(z-h)^2\right]dz\right)} & \lambda\leq\frac{\sigma}{2} \\ & \lambda>h\end{cases} \tag{21}$$

With the above equation, $\overline{G}$ may be determined up to $\lambda=\sigma/2$ when a suitable representation of $\rho\left(z\right)$ is provided. Additionally, Eq. 21 confirms that $\overline{G}$ is continuous at $\lambda=h$, provided that $\lambda\leq\sigma/2$.

Equation 21 also provides exact information about the limit of $\overline{G}$ as the cavity initially grows. For example, taking the limit of $\overline{G}$ as $\lambda\to0$ (which necessarily implies $\lambda\leq h$), we find that

$$\lim_{\lambda\to0}\overline{G}\left(\lambda,h\right)=\frac{\rho\left(h\right)}{\rho}, \tag{22}$$

which differs from the $h\leq0$ case where $\overline{G}\left(-h,h\right)=p/\rho kT$[20]. (For $h=0$, these results are identical as $\rho\left(0\right)=p/kT$.) As $h\to\infty$, i.e., we are growing the cavity within a bulk fluid, we recover the SPT result of $\overline{G}\left(0,\infty\right)=1$ since $\rho\left(h\right)\to\rho$ at a sufficient distance from the hard wall. Equation 22 does align with our intuition regarding cavity growth, since one expects the limiting stress normal to a cavity of zero radius to equal the local density of the HS fluid multiplied by kT.

A second limiting property of $\overline{G}$ obtained from Eq. 21 for $h>0$ is

$$\lim_{\lambda\to0}\frac{\partial\overline{G}}{\partial\lambda}=0, \tag{23}$$

which is quite different from the initially negative slope of $\overline{G}$ for $h\leq0$[20], though identical to the $\lambda\to0$ limit of $\partial G/\partial\lambda$ for bulk SPT. This difference follows from the fully spherical shape of the cavity for $\lambda<h$, manifested by the nonzero lower bounds of the integrals in Eq. 21. Since the limiting slope of $\overline{G}$ is zero, it is unclear whether $\overline{G}$ increases or decreases for λ infinitesimally larger than zero. Proceeding to the second derivative of $\overline{G}$, however, one finds that

$$\lim_{\lambda\to0}\frac{\partial^2\overline{G}}{\partial\lambda^2}=\frac{1}{3\rho}\left.\frac{\partial^2\rho\left(z\right)}{\partial z^2}\right|_{z=h}, \tag{24}$$

which may be positive, negative, or even zero, since the curvature of $\rho\left(z\right)$ varies between positive and negative concavity. Hence, the curvature of $\rho\left(z\right)$ at $z=h$ controls the initial

12

behavior of $\overline{G}$ for $h > 0$, positive curvature leading to an initial increase in $\overline{G}$ and vice versa. As noted before, $\overline{G}$ behaves quite differently from the bulk $G(\lambda)$, which is always a monotonically increasing function of λ.

We may also examine the discontinuity in $\partial\overline{G}/\partial\lambda$ at $\lambda = h$ for $\lambda \le \sigma/2$. After differentiation of Eq. 21, we find that

$$\Delta\left[\frac{\partial\overline{G}}{\partial\lambda}\right]_{\lambda=h} = \frac{\int_0^{2h}\rho(z)dz}{4\rho h^2\left(1 - \pi\int_0^{2h}\rho(z)z\,[2h-z]\,dz\right)} - \frac{\rho(0)}{2\rho h\left(1 - \pi\int_0^{2h}\rho(z)z\,[2h-z]\,dz\right)}$$

$$= \frac{1}{2h}\left[\overline{G}(h,h) - G(h,\pi,h)\right] \qquad\qquad \lambda \le \sigma/2, \qquad\qquad (25)$$

where the second line follows from various relations provided in Refs. [21, 22]. Comparison of Eqs. 16 and 25 reveals that $\partial G(\lambda,\theta,h)/\partial\lambda$ is continuous at $\lambda = h$, so that the integral term in Eq. 16 vanishes, provided that $\lambda \le \sigma/2$. Lastly, since $\overline{G} \le p/\rho kT$[20] and $G(h,\pi,h) \ge p/\rho kT$[21, 22] (where we note that $\rho(0)/\rho = p/kT$ and the denominator in the expression for $G(h,\pi,h)$ is less than unity), this discontinuity in $\partial\overline{G}/\partial\lambda$ is negative. For $\lambda > \sigma/2$, we cannot definitively say that $\partial G(\lambda,h,\theta)/\partial\lambda$ is continuous at $\lambda = h$ and, consequently, the discontinuity in $\partial\overline{G}/\partial\lambda$ could be positive. For further discussion, see Appendix B of Ref. [45].

Additional exact conditions on $\overline{G}$ can be obtained by considering the behavior of $\overline{G}$ at $\lambda = \sigma/2$. Using Eq. 18, examination of the exact form of $\overline{G}$ for $\lambda = \sigma/2 - \epsilon$ and $\lambda = \sigma/2 + \epsilon$, with $\epsilon \to 0$, indicates that $\overline{G}$ is continuous up to the first derivative with respect to λ at $\lambda = \sigma/2$, as was the case previously[20]. This is not the case, though, when $h = \sigma/2$. Here, $\lambda = \sigma/2$ coincides with $\lambda = h$, so that Eq. 25 must apply and only $\overline{G}$ itself is continuous. A condition on the second derivative of $\overline{G}$ can also be obtained, though which proves more difficult to apply. In Eq. 20 we expect Ω_2 to supply a divergent third derivative of F_2 with respect to λ as $\lambda \to \sigma/2^+$ as noted previously[22], implying that $\partial^2\overline{G}/\partial\lambda^2 \to -\infty$ as $\lambda \to \sigma/2^+$ for $h > 0$. For $h = \sigma/2$, additional finite terms would appear upon further differentiation of Eq. 16, but the behavior of F_2 still suggests that the divergence of $\partial^2\overline{G}/\partial\lambda^2$ to $-\infty$ should persist. These conditions complete the set of conditions on $\overline{G}$ that may be derived using solely statistical geometric arguments. Like all previous versions of SPT, we now appeal to macroscopic thermodynamics to provide additional information about $\overline{G}$.

C. Conditions on $\overline{G}(\lambda, h)$ for $\lambda > \sigma/2$

In Ref. [20], three exact conditions on $\overline{G}$ for $\lambda > \sigma/2$ were identified for $h \leq 0$. An additional exact condition was available for $h = 0$ only, necessitating a semi-empirical condition relating the $\overline{G}$ interpolation for $h < 0$ to the hemispherical ($h = 0$) case. An aforementioned exact condition related to γ_∞ was derived later[22], becoming the fifth exact condition of I-SPT for $h \leq 0$. The net result is that different sets of conditions on $\overline{G}$ become available for different values of h, which is again the case for $h > 0$.

1. Exact Conditions

The connection between SPT and macroscopic thermodynamics provides several exact conditions on $\overline{G}$. For finite h and large enough values of λ, the cavity eventually intersects the $z = 0$ plane. As shown in Ref. [29], the reversible work of growing a cavity that intersects a planar wall is given by

$$W = pV(\lambda, h) - \gamma_\infty A_{wall}(\lambda, h) + \gamma_\lambda A(\lambda, h) + \tau_\lambda L(\lambda, h), \qquad (26)$$

where $V(\lambda, h) = \pi (2\lambda^3 + 3\lambda^2 h - h^3)/3$ is the volume of the cavity that develops beyond the wall ($z = 0$ plane), $A_{wall} = \pi (\lambda^2 - h^2)$ is that portion of the wall covered by the cavity, γ_λ is the surface tension of the cavity of radius λ when it is placed far away from the wall (and the dividing surface is coincident with the surface of the cavity), τ_λ is the line tension of the cavity and $L(\lambda, h) = 2\pi (\lambda^2 - h^2)^{1/2}$ is the linear interface generated by the intersection of the cavity and the wall. Using either Eq. 9 or Eq. 17, differentiation of Eq. 26 once with respect to λ shows that[20]

$$\lim_{\lambda \to \infty} \overline{G}(\lambda, h) = \frac{p}{\rho kT}, \qquad (27)$$

which requires that the average normal stress on the cavity surface equal the system pressure as $\lambda \to \infty$. Differentiating W a second time reveals that [22]

$$\lim_{\lambda \to \infty} \left[\lambda^2 \frac{\partial \overline{G}(\lambda, h)}{\partial \lambda} \right] = -\frac{\gamma_\infty}{\rho kT}. \qquad (28)$$

When a Laurent series is introduced to interpolate $\overline{G}$ for macroscopic radii, Eqs. 27 and 28 are used to determine the first two interpolation coefficients, respectively. Another condition that follows from Eq. 26 is the requirement that W not contain terms proportional to $\ln \lambda$

14

as $\lambda \to \infty$[48], which can be satisfied through an appropriate choice of the I-SPT interpolation function. Lastly, Widom's inverse potential distribution theorem (or, equivalently, the invariance of the chemical potential in an equilibrium nonuniform fluid) requires[49, 50]

$$\frac{\rho\left(\mathbf{r}_1\right)}{\rho\left(\mathbf{r}_2\right)} = \exp\left[\frac{W\left(\mathbf{r}_2\right) - W\left(\mathbf{r}_1\right)}{kT}\right] , \tag{29}$$

where $\rho\left(\mathbf{r}_i\right)$ is the local density of HS at position $\mathbf{r}_i$ and $W\left(\mathbf{r}_i\right)$ is the reversible work of inserting a HS at that same location. Application of the above to the nonuniform density that develops near the wall (noting again that $\lambda = \sigma$ is equivalent to another HS solvent particle), we conclude that

$$\exp\left[\frac{\mu^{ex} - W\left(\sigma, h\right)}{kT}\right] = \frac{\rho\left(h\right)}{\rho} , \tag{30}$$

where μ^{ex} is the excess chemical potential of the HS fluid, i.e., the work of inserting a HS within the bulk fluid far away from the wall. The above equation constrains the integral of $\overline{G}$ up to $\lambda = \sigma$ (through Eq. 12) as opposed to restricting $\overline{G}$ itself.

2. Pseudo-Exact Conditions

While several exact conditions on $\overline{G}$ can be invoked, our initial attempts to describe $\overline{G}$ revealed that additional conditions were needed to generate interpolations that were reliable over large ranges of both λ and h. Another condition, for example, follows from noting that the reversible work of inserting a cavity is path-independent. Consequently, one may write the work of growing a cavity in terms of either $\overline{F}\left(\lambda, h\right)$ or $\overline{G}\left(\lambda, h\right)$. So, for a cavity of radius $\lambda = h$ located at h, $W\left(h, h\right)$ is formally equal to

$$W\left(h, h\right) = 4\pi kT \int_0^h \overline{G}\left(r, h\right) r^2 dr = 2\pi kTh^2 \int_{-h}^h \overline{F}\left(\lambda, h\right) dz. \tag{31}$$

Of course, $\overline{F}\left(\lambda, h\right)$ is approximated over most of its domain, so the application of Eq. 31 is an approximate condition that becomes dependent on the accuracy of the interpolations describing $\overline{F}\left(\lambda, h\right)$. Nevertheless, the predictions of $W\left(\lambda, h\right)$ obtained from $\overline{F}\left(\lambda, h\right)$ were shown to be quite accurate (in comparison with W obtained via molecular simulation), so this condition may be considered as pseudo-exact. This relation is only useful for $h > \sigma/2$, though, since $W\left(h, h\right)$ is known exactly for smaller h and is equal to zero for $h < 0$. (As a note of interest, we point out that this condition makes an interpolation of $\overline{G}$ for $h > 0$

15

dependent on the interpolation for $\overline{G}$ at $h = 0$ since $W(\lambda, h = 0)$ is itself a condition on $\overline{F}$[22].)

Another condition may be again obtained from Eq. 26. Given that γ_λ can be expanded in inverse powers of λ about γ_∞ as follows[29]

$$\gamma_\lambda = \gamma_\infty \left(1 - \frac{2\delta_\infty}{\lambda} + \cdots \right), \tag{32}$$

in which δ_∞ is the Tolman length[51], one finds that

$$\lim_{\lambda \to \infty} \left[\frac{\lambda^2}{2} \frac{\partial}{\partial \lambda} \left(\lambda^2 \frac{\partial \overline{G}(\lambda, h)}{\partial \lambda} \right) \right] = \tau_\infty - 2\gamma_\infty \delta_\infty , \tag{33}$$

where τ_∞ is the limiting value of the line tension as $\lambda \to \infty$. If a Laurent series is used to interpolate $\overline{G}$, the above can be used to determine one of the interpolation coefficients. Both γ_∞ and δ_∞ can be determined from an accurate version of bulk SPT, as was developed, for example, in Ref. [42], and can be considered as (almost) exactly known. τ_∞, however, has not been previously obtained for the HS fluid, the form of which and its relation to other surface thermodynamic properties having only been properly derived in Ref. [29]. One complication that arises concerning the use of Eq. 33 is that τ_∞ could be a function of h, and so it is not known in general. In fact, one would normally invoke Eq. 33 to predict the values of τ_∞ from some version of I-SPT, rather than impose Eq. 33 as a condition within I-SPT. But, various physical and geometric arguments put forth in Ref. [29] strongly suggest (though do not prove) that τ_∞ is independent of h. For finite values of h, all cavities intersecting the wall eventually approach a hemispherical cavity as $\lambda \to \infty$. Since an accurate expression for $\overline{G}$ already exists for $h = 0$, we therefore compute τ_∞ for the hemispherical case (evaluating W for the hemisphere and applying Eq. 26 as $\lambda \to \infty$) and then assume that this τ_∞ applies to all other values of h. The accuracy of the results, including the need to impose Eq. 33 as another condition, provide an indirect test of the assumption that τ_∞ is not a function of h.

3. An Approximate Condition

The final condition that we introduce is an approximation of the value of $\overline{G}(h, h)$ for $h > \sigma/2$. [$\overline{G}(h, h)$ is known exactly for $h \leq \sigma/2$.] Some approximate knowledge of $\overline{G}(h, h)$ was found to greatly assist in fitting $\overline{G}(\lambda, h)$ for any h larger than about σ. Among the conditions discussed above, the only one relevant to $\lambda > \sigma$ while not in the limit of $\lambda \to \infty$

16

is Eq. 31, which constrains the integral of $\overline{G}(\lambda, h)$ up to $\lambda = h$ rather than the value itself. Consequently, an interpolation of $\overline{G}$ that does not include some information about $\overline{G}(h, h)$ directly could produce an unreasonable value of $\overline{G}(h, h)$, impacting the calculation of W for $\lambda > h$. [We observed, for example, that interpolations without a condition on $\overline{G}(h, h)$ usually predicted values of $\overline{G}(h, h)$ well below those found from simulation. In turn, predictions of W for $\lambda > h$ fell unacceptably below simulation results.] To generate a condition for $\overline{G}(h, h)$, we follow Ref. [40], in which the potential distribution theorem[49, 50] is again utilized to relate the local density of HS centers at a given θ on the cavity surface to the reversible work of inserting a HS particle or an equivalent σ-sized cavity. Using Eq. 29, one can show that

$$\overline{G}(h, h) = \frac{p}{2\rho kT} \int_0^\pi \exp\left[\frac{W_\sigma(\mathbf{r}_{ref}) - W_\sigma(\lambda, \theta, h)}{kT}\right] sin\theta d\theta \ , \tag{34}$$

where $W_\sigma(\lambda, \theta, h)$ is the work of inserting a HS or growing a cavity of radius σ at the specified position and $W_\sigma(\mathbf{r}_{ref})$ is the work of inserting a HS at a location far away from the λ-sized cavity but whose center resides at the $z = 0$ plane (where the local density of HS is $p/\rho kT$). Equation 34 is formally exact, although W_σ is not rigorously known in general. Thus, an approximate expression for W_σ must be used. We compute the various components of W_σ using a "surface thermodynamic" approximation, which is discussed in detail in the Appendix. Our present approximation is similar in inspiration to the "ideal gas approximation" invoked in Ref. [40] to provide a sixth condition for bulk SPT, but is higher order in that it incorporates more accurate thermodynamic information about the cavity. The resultant approximation for $\overline{G}(h, h)$ is quite accurate up to $\rho\sigma^3 = 0.65$, though it produces poor predictions thereafter. Numerical results for our approximated $\overline{G}(h, h)$ are discussed later in the paper.

D. Summary of Conditions on $\overline{G}(\lambda, h)$

In all, 10 conditions (most exact) are employed to constrain the form of $\overline{G}(\lambda, h)$ for λ greater than its upper exact limit. As a summary, the conditions on $\overline{G}(\lambda, h)$ used by I-SPT are:

1. $\overline{G}(\lambda, h)$ is continuous at its exact limit, $\lambda = \sqrt{h^2 + (\sigma/2)^2}$ for $h < 0$ and $\lambda = \sigma/2$ for $h \geq 0$

2. $\partial \overline{G}/\partial \lambda$ is continuous at its exact limit, except for $h = \sigma/2$

3. $\partial \overline{G}/\partial \lambda$ at $\lambda = \sigma/2^+$ is known exactly for $h = \sigma/2$

4. $\overline{G}(\lambda, h)$ is continuous at $\lambda = h$

5. $\overline{G}(h, h)$ is computed approximately via Eq. 34

6. $\exp\left[(\mu^{ex} - W(\sigma, h))/kT\right] = \rho(h)/\rho$

7. $W(h, h) = 2\pi\rho kTh^2 \int_{-h}^{h} \overline{F}(h, z)\, dz$

8. $\lim_{\lambda \to \infty} \overline{G}(\lambda, h) = p/\rho kT$

9. $\lim_{\lambda \to \infty} \left[\lambda^2 \partial \overline{G}(\lambda, h)/\partial \lambda\right] = -\gamma_\infty/\rho kT$

10. $\lim_{\lambda \to \infty} \left[(\lambda^2/2)\, \partial\left(\lambda^2 \partial \overline{G}(\lambda, h)\right)/\partial \lambda\right] = (\tau_\infty - 2\gamma_\infty \delta_\infty)/\rho kT$

E.   Interpolation Functions for $\overline{G}(\lambda, h)$

As in previous forms of SPT and I-SPT, we require an interpolation function to represent $\overline{G}$ for values of λ outside the exact domain. The form of this interpolation for $\lambda \geq h$ is again suggested by the surface thermodynamics of macroscopic cavities. Surface thermodynamics does not, however, state anything definitively about the form of $\overline{G}$ for $\sigma/2 \leq \lambda \leq h$ (which is only relevant for $h > 0$). In addition, since $\overline{G}$ has a discontinuous first derivative at $\lambda = h$, an approximate representation of $\overline{G}$ should be based on the combination of two separate functions, one for $\sigma/2 \leq \lambda \leq h$ and the other for $\lambda \geq h$, both of which become equal at $\lambda = h$. So while the interpolation function for $\lambda \geq h$ is more or less dictated by surface thermodynamics, we are free to select an appropriate interpolation for $\lambda \leq h$.

In Ref. [29], the limiting form of dW for macroscopic cavities ($\lambda \to \infty$) that intersect the wall was shown to be given by the following expansion

$$dW = 2\pi P\lambda(\lambda + h)d\lambda + \pi\gamma_\infty(2\lambda + h)d\lambda + \phi_1(\rho, h)d\lambda + \frac{\phi_2(\rho, h)}{\lambda^2}d\lambda + \cdots \qquad (35)$$

where $\phi_i(\rho, h)$ is a function of ρ and h only. The above indicates that $\overline{G}$ must expand as

$$\overline{G}(\lambda, h) = \psi_o(\rho) + \psi_1(\rho)\frac{(2\lambda + h)}{\lambda(\lambda + h)} + \frac{\psi_2(\rho, h)}{\lambda(\lambda + h)} + \frac{\psi_4(\rho, h)}{\lambda^3(\lambda + h)} + \cdots \qquad (36)$$

18

in which only the coefficients ψ_o and ψ_1 are functions of ρ, while all higher-order coefficients are also functions of h. A more convenient expansion of $\overline{G}$ can be obtained from Eq. 36 (which appears in Ref. [45]) after some straightforward algebra

$$\overline{G}(\lambda, h) = \beta_0(\rho) + \frac{\beta_1(\rho)}{\lambda} + \frac{\beta_2(\rho)}{\lambda(\lambda + h)} + \frac{\beta_4(\rho, h)}{\lambda^3(\lambda + h)} + \frac{\beta_5(\rho, h)}{\lambda^4(\lambda + h)} + \cdots, \qquad (37)$$

where after invoking some of the previously derived limiting conditions on $\overline{G}$ we find that

$$\beta_0(\rho) = \psi_o(\rho) = \frac{P}{\rho kT}$$

$$\beta_1(\rho) = 2\psi_1(\rho) = \frac{\gamma_\infty}{\rho kT}$$

$$\beta_2(\rho) = \psi_2(\rho, h) - h\psi_1(\rho) = \frac{\tau_\infty - 2\gamma_\infty \delta_\infty}{\rho kT}$$

$$\beta_i(\rho, h) = \psi_i(\rho, h) \qquad i \geq 4 . \qquad (38)$$

$\beta_2(\rho)$ is listed as only being a function of ρ, since, as noted earlier, arguments provided in Ref. [29] strongly suggest that τ_∞ is independent of h. Again no term containing $\lambda^2(\lambda + h)$ appears in the denominator, which would lead to an unphysical logarithmic contribution to W as $\lambda \to \infty$[48]. Equation 37 differs slightly from the interpolation in Ref. [20], but is the proper limiting form of $\overline{G}$. (Ref. [20] did not rely upon the correct expansion of dW that now appears in Ref. [29].) Strictly speaking, Eq. 37 is only valid in the large cavity limit, but, like bulk SPT, we again apply this interpolation function to microscopic cavity sizes for $\lambda \geq h$.

The surface thermodynamic analysis that leads to Eq. 37 does not provide any definite suggestions concerning the form of $\overline{G}$ for $\lambda \leq h$. In fact, the properties of these completely spherical cavities are not in general well understood since they are neither "bulk" cavities in a uniform fluid nor do they intersect the planar wall at $z = 0$. Hence, a Laurent series interpolation for $\overline{G}$ does not necessarily apply for $\lambda \leq h$. We note, however, that for values of h far from the wall, where the HS fluid density profile is uniform and equal to ρ, $W(\lambda, h)$ should be identical to the bulk SPT value of $W(\lambda)$, at least until λ is large enough such that some portion of the HS fluid surrounding the cavity begins to "feel" the presence of the wall at $z = 0$. In practice, h does not need to be exceedingly large before a small enough cavity views its immediate environment as being that of a bulk system. For example, even for a bulk density of $\rho\sigma^3 = 0.914$, the HS density profile is uniform about 7σ away from the

wall. At such a high density and h position, even small cavities could be well-described by the bulk SPT relation.

Outside of requiring that $\overline{G}$ for $\lambda \leq h$ mimic to some extent bulk SPT properties for large enough values of h, this condition does not provide a generally valid form of $\overline{G}$, since bulk behavior can no longer be invoked for small h or for values of λ approaching h (from below) where one side of the cavity is close enough to the hard wall. In the absence of a suggested form of the interpolation, we nevertheless propose that a simple Laurent series still be used to approximate $\overline{G}$ for $\sigma/2 < \lambda \leq h$. For one, a Laurent series ensures that $W(\lambda, h)$ is composed of terms proportional to λ^3, λ^2, etc., that are associated with volume and surface-area contributions to W. Additionally, this matches the similar known form of W for the growth of bulk cavities at large h. Also, the use of just one additional function, instead of multiple functions within the same range, greatly simplifies the entire interpolation scheme required by I-SPT. Therefore, we choose to interpolate $\overline{G}$ for $\sigma/2 < \lambda \leq h$ by

$$\overline{G}(\lambda, h) = \xi_0(\rho, h) + \frac{\xi_1(\rho, h)}{\lambda} + \frac{\xi_2(\rho, h)}{\lambda^2} + \frac{\xi_4(\rho, h)}{\lambda^4} + \cdots, \tag{39}$$

where all the series coefficients ξ_i are floating parameters dependent on both ρ and h. This dependence on h follows from the various conditions on $\overline{G}$, which are functions of ρ and h and so are not necessarily equal to the analogous coefficients of the bulk $G(\lambda)$. Note that Eq. 39 does not include a term proportional to λ^{-3}, which would yield a logarithmic term in W. The suppression of a logarithmic term in W is not strictly required since it would not be dependent on λ for $\lambda > h$. But, to ensure that $\overline{G}(\lambda, h)$ becomes identical to the bulk fluid $G(\lambda)$ for $h \gg 0$, our chosen interpolation of $\overline{G}$ for $\sigma/2 < \lambda \leq h$ does not contain such a term.

Assembling the interpolation function(s) for a particular h requires some effort since the conditions listed in subsection III D are not applicable to every value of h or to the subdomains of λ. Table I contains a summary that lists the ranges of h, each of which is given a "Region" number, and the set of conditions applicable to that Region. Additionally, the table lists which conditions apply to each subdomain of λ, $\sigma/2 \leq \lambda \leq h$ and $\lambda \geq h$ (for $h > 0$). The number of conditions applicable to each subdomain of λ determines the number of fitting conditions available for the interpolation for each subdomain (Eqs. 37 and 39). As an example, the table indicates that for $h = 3\sigma/4$ (Region V), eight conditions are available, from which we compute $(\xi_0, \xi_1, \xi_2, \xi_4)$ and $(\beta_0, \beta_1, \beta_2, \beta_4, \beta_5)$.

h-domain	Region Name	Number of available conditions	Interpolation Conditions for:	Interpolation Conditions for:
			-	$\lambda \geq \sqrt{h^2 + (\sigma/2)^2}$
$h < 0$	I	5	-	1*, 2*, 8, 9, 10
			$\sigma/2 \leq \lambda \leq h$	$\lambda \geq h$
$h = 0^\dagger$	II	5	-	1, 2, 6, 8, 9
$0 \leq h < \sigma/2$	III	6	-	1, 2, 6, 8, 9, 10
$h = \sigma/2$	IV	6	-	1, 3, 6, 8, 9, 10
$\sigma/2 < h < \sigma$	V	$8^\ddagger$	1, 2, 5, 7	5, 6, 8, 9, 10
$h = \sigma$	VI	$7^\ddagger$	1, 2, 5, 6	5, 8, 9, 10
$h > \sigma$	VII	$8^\ddagger$	1, 2, 5, 6, 7	5, 8, 9, 10

TABLE I: Summary of the interpolation scheme for $\overline{G}(\lambda, h)$ for all possible h-domains. Column two connects the h-domain to the "Region Name" used in the text. Columns three, four, and five give the number of conditions for each h-domain and lists those conditions by their identification numbers used in Section III D.

*For $h < 0$, conditions 1 and 2 are the continuity of $\overline{G}$ and $\partial\overline{G}/\partial\lambda$ at $\lambda = \sqrt{h^2 + (\sigma/2)^2}$, respectively.

† The interpolation for $\overline{G}$ for $h = 0$ provides τ_∞ and, hence, condition 10 is satisfied automatically.

‡Since condition 5 appears in both interpolations, the count in columns three and four does not add up to the number in column two

IV. RESULTS

Using the above mentioned interpolations of and conditions on $\overline{G}$, values of $\overline{G}$ and, thereby, W for a variety of HS bulk fluid densities can be computed and compared to results obtained from molecular simulation. As discussed previously, the determination of $\overline{G}$ requires information about $\rho(z)$, either by an approximation or direct simulation measure. $\rho(z)$ may be generated in a number of ways, including direct measurement by molecular simulation[20, 22], theoretical approximations[52–55], and statistical mechanical density functional theory using a nonlocal HS functional[56–58]. Here, we calculated $\rho(z)$ using Monte Carlo simulation, as was done in the previous I-SPT papers[20–22]. $\overline{G}$

was determined within the exact domain via a straightforward numerical integration of the simulation-generated $\rho(z)$ according to Eq. 21. HS thermodynamic properties (e.g., p, γ_∞, γ_λ, and δ_∞ as functions of the bulk density ρ) were computed via the thermodynamically consistent version of SPT that invokes the Carnahan-Starling-based[44] version of SPT (CS-SPT$_M$)[41, 42]. τ_∞ was determined from Eq. 26 and various relations contained within Ref. [29], which requires input from I-SPT for a hemisphere ($h = 0$) as well as these same bulk spherical cavity results again obtained with CS-SPT$_M$.

All relevant simulation data were generated via the Monte Carlo (MC) method within the isothermal-isobaric ensemble (constant N, p, T, where N is the number of particles) with hard walls in one direction (arbitrarily designated as the z-direction) and periodic boundary conditions in the other two directions. Both $\rho(z)$ and $W(\lambda, h)$ were determined using the simulation methods described in Refs. [20] and [22]. $W(\lambda, h)$ profiles were determined for $h = 0.25\sigma$, 0.5σ, 0.75σ, σ, 1.25σ, and 3σ. For comparison at certain h and $\rho\sigma^3$, $\overline{G}(\lambda, h)$ was computed from simulation measurements of W. To obtain $\overline{G}(\lambda_0, h)$ from W, we fit W in the vicinity of λ_0 to a polynomial and entered $\partial W / \partial \lambda$ from the regression function into Eq. 17 (using $W = -kT \ln P_0$).

A.   Approximation of $\overline{G}(h, h)$

In order to validate the surface thermodynamic approximation that was invoked in Eq. 34 (also see the Appendix) when generating another condition on $\overline{G}$, we also determined the values of $\overline{G}(h, h)$ from simulation for different bulk fluid densities. $\overline{G}(h, h)$ was computed indirectly from simulation in the following manner. First, $W(\lambda, h)$, which was directly calculated from the simulation, was fit to a third-order polynomial over the domain $h - 0.1\sigma < \lambda < h + 0.1\sigma$. Then, $\overline{G}$ was determined by taking the derivative of the resulting fit of W with respect to λ. Values of $\overline{G}(h, h)$ for five bulk densities and a few representative values of h are provided in Table II. (Note that $\overline{G}(\lambda, h)$ is continuous at $\lambda = h$, so that W and its first derivative are also continuous at this same point. Thus, W can be fit to a completely smooth function across $\lambda = h$ if only information about $\overline{G}(h, h)$ is required. This approach cannot, of course, yield information about the apparent discontinuity in the first derivative of $\overline{G}$ at $\lambda = h$.)

The approximation for $\overline{G}(h, h)$ is quite accurate for the three lowest densities considered,

h/σ	$\rho\sigma^3 = 0.3$		$\rho\sigma^3 = 0.5$		$\rho\sigma^3 = 0.6$		$\rho\sigma^3 = 0.7$		$\rho\sigma^3 = 0.85$	
	Sim.	I-SPT	Sim.	I-SPT	Sim.	I-SPT	Sim.	I-SPT	Sim.	I-SPT
0.75	1.583	1.588	2.007	2.125	2.432	2.532	2.766	3.502	3.392	16.635
1	1.682	1.675	2.486	2.368	2.853	2.929	3.466	4.199	4.318	17.602
1.25	1.735	1.729	2.609	2.524	3.289	3.177	3.803	4.577	5.064	16.853
3	1.874	1.863	2.956	2.926	3.790	3.792	-	5.308	-	12.741
$\frac{p}{\rho kT}$	1.967		3.262		4.283		5.710		9.099	

TABLE II: Values of $\overline{G}(h,h)$ computed by MC simulation (marked "Sim.") and the surface thermodynamic approximation in Eq. 34 (marked "I-SPT") for several densities below the freezing transition and h where the approximation is used to interpolate $\overline{G}(\lambda, h)$. The value of $\overline{G}(\infty, h) = p/\rho kT$ is also provided in the last row. $\overline{G}(h,h)$ should not exceed $p/\rho kT$, and we find that the surface thermodynamic approximation does predict $\overline{G}(h,h) > p/\rho kT$ for $\rho\sigma^3 > 0.74$.

differing from the simulation results by no more than 6%. Common among these three lowest densities is that the approximation overpredicts $\overline{G}(h,h)$ for small h (particularly $h < \sigma$), though it is quite close to the simulation values for larger h. At $h = 3\sigma$, the approximation for $\overline{G}(h,h)$ is within 1% of the simulation value for $\rho\sigma^3 = 0.3$, 0.5, and 0.6. That our approximation becomes more accurate as h increases is unsurprising, as the approximation used in Eq. 34 will automatically yield $\overline{G}(h,h) = p/\rho kT$ in the limit of $h \to \infty$ (see the Appendix), which is of course identical to the limiting value of $\overline{G}(\lambda, h)$ itself.

For the largest densities, $\rho\sigma^3 = 0.7$ and 0.85, the approximation, however, breaks down quite suddenly, overpredicting $\overline{G}(h,h)$ for all values of h while incorrectly predicting that $\overline{G}(h,h) > p/\rho kT$ for $\rho\sigma^3 = 0.85$ (while there is no rigorous proof requiring that $\overline{G}$ always remain less than $p/\rho kT$, surface thermodynamics strongly suggests that for large cavities $\overline{G}$ should approach $p/\rho kT$ from below; in addition, simulation has so far only shown that $\overline{G} \leq p/\rho kT$). A more detailed analysis (not shown here) reveals that the approximation yields $\overline{G}(h,h) > p/\rho kT$ for $\rho\sigma^3 > 0.74$, which provides a strict upper limiting density on the validity of the approximation. In practice, though, the approximation begins to predict $\overline{G}(h,h)$ unreliably for $\rho\sigma^3 \gtrsim 0.65$. For smaller ρ, the approximation for $\overline{G}(h,h)$ is quite reliable and so can be used for the computation of W via I-SPT. Note that $\overline{G}(h,h)$ is known

exactly for $h \leq \sigma/2$, so accurate results are obtained for all HS fluid densities at these values of h.

B. Comparison of $\overline{G}(\lambda, h)$ and $W(\lambda, h)$ Predictions to Simulation for $h > 0$

To provide a basis for comparison and for identifying interesting features in $\overline{G}(\lambda, h)$ at $h > 0$, Figs. 2 and 3 plot $G(\lambda, h = 0)$ and $\overline{G}(\lambda, h = 0)$, respectively for reduced densities between 0.2 and 0.7, and Fig. 4 compares $W(\lambda, h = 0)$ for $\rho\sigma^3 = 0.3$, 0.5, and 0.6 obtained from both I-SPT and MC simulations. Similar plots have already been extensively discussed[20], but we again highlight the important aspects of $\overline{G}(\lambda, h = 0)$: it has an initial value of $p/\rho kT$, immediately decreases to its minimum value at $\lambda < \sigma/2$, and then increases asymptotically toward $p/\rho kT$ as $\lambda \rightarrow \infty$.

We begin our examination of I-SPT predictions with a comparison of simulation and theoretical results for $h = 0.25\sigma$, which utilizes the interpolation for Region III. Figure 5 contains plots of $\overline{G}(\lambda, 0.25\sigma)$ for reduced densities between 0.2 and 0.7, in which $\overline{G}$ is exactly known for $\lambda \leq \sigma/2$. The most obvious feature of the plot is the discontinuous slope of $\overline{G}$ at $\lambda = h = 0.25\sigma$, which becomes more noticeable as ρ increases. The change in slope at $\lambda = h$ for this value of h is always negative, which agrees with the prediction from the exact analysis of $\overline{G}(\lambda, h)$. (Furthermore, this result implies that $G(h, \pi, h) > \overline{G}(h, h)$, verifying the intuitive arguments presented earlier.) We also observe that $\overline{G}(0, 0.25\sigma)$ is much less than $p/\rho kT$, as anticipated by the exact analysis. Yet, $\overline{G}(0, 0.25\sigma) > 1$ in all cases, a required result since $\rho(0.25\sigma) > \rho$ for the density profiles associated with these ρ (see Eq. 22). The reduction in $\overline{G}(0, 0.25\sigma)$ compared to the hemispherical case is representative of the decrease in $\rho(z)$ between $z = 0$ and $z = 0.25\sigma$. From $\lambda = 0$ to h, $\overline{G}$ increases monotonically. Yet, the discontinuity in $\partial\overline{G}/\partial\lambda$ at $\lambda = h$ is sufficiently negative to yield a sign change in the slope so that a sudden and short-ranged decrease in $\overline{G}$ occurs before it resumes a monotonic increase. The decrease in $\overline{G}$ is relatively small in all cases, with, for example, an absolute total decrease of only 0.013 for $\rho\sigma^3 = 0.7$. After the discontinuity, the asymptotic increase in $\overline{G}$ is very similar to that of the hemispherical case, effectively reaching the limiting value of $p/\rho kT$ by $\lambda = 5\sigma$. The similarity between $\overline{G}$ at any h and the hemispherical $\overline{G}$ interpolation at large cavities is not surprising, since the first two terms in the corresponding interpolations are identical (deviations appear at the term proportional

to β_2 and higher).

Figure 6 contains predictions of $W(\lambda, h)$ for $h = 0.25\sigma$ at $\rho\sigma^3 = 0.3, 0.5$, and 0.6, obtained both from I-SPT and MC simulations. On the scale of the plot, there is no discernible difference between these two sets of results, confirming that $\overline{G}$ is well-represented by our chosen interpolation scheme. For $\rho\sigma^3 = 0.3$, the I-SPT values of W differ from simulation values by no more than $0.31kT$ up to $\lambda = 3\sigma$. Between $\lambda = \sigma/2$ and 3σ, the relative difference is typically less than 1%, reaching 3% for only a small range of cavity radii. A similar pattern is observed for $\rho\sigma^3 = 0.5$ and 0.6, where the absolute error is less than $0.2kT$ for $\rho\sigma^3 = 0.5$ and less than kT for $\rho\sigma^3 = 0.6$. In relative terms, these differences are less than 2.5%. The values of W for $\rho\sigma^3 = 0.5$ are particularly accurate, falling within 0.5% of the simulation points for $2\sigma < \lambda < 3\sigma$. For these three densities, the errors are small enough to be considered statistically insignificant, given that estimates of the standard deviations of the values of W computed from simulation are around 1.5-2%. Based on the rapid convergence of $\overline{G}$ to its asymptotic value, we expect the accuracy of W to continue for larger λ, and any error should continue to decrease relative to simulation. Comparison with the hemispherical work values, $W(\lambda)$, also indicates that $W(\lambda, 0.25\sigma)$ usually exceeds $W(\lambda, 0)$ and is always larger in the limit of $\lambda \to \infty$, a consequence of the extra volume the cavity possesses when centered at $h > 0$. For $\rho\sigma^3 = 0.6$, $W(\lambda, 0)$ is larger than $W(\lambda, 0.25\sigma)$ for very small radii ($< 0.2\sigma$), which follows from the sharp reduction in $\overline{G}$ around $\lambda = 0$ relative to the hemisphere that cannot be overcome at these radii by the larger cavity volume.

The examination of the I-SPT predictions becomes more interesting for larger h, where the conditions at $\lambda = h$ are now required. Figure 7 contains $\overline{G}(\lambda, h)$ plotted for $h = 0.75\sigma$ (Region V). Much of the discussion regarding the qualitative structure of $\overline{G}$ for $h = 0.25\sigma$ applies verbatim to $h = 0.75\sigma$. The most noticeable new feature in $\overline{G}$ is the sudden change in shape at $\lambda = h$ for $\rho\sigma^3 = 0.7$, where the slope decreases abruptly, though stays (barely) positive. Based on Table II and the associated discussion, however, this is an artifact of the condition on $\overline{G}(h, h)$, which is overpredicted at this higher density. Consequently, we surmise that the proper shape of $\overline{G}$ for $\rho\sigma^3 = 0.7$ is more like the other densities in the plot, and that we should not consider the predicted $\overline{G}$ (and, in turn, W) to be especially accurate for this density. A more detailed examination of the discontinuous change in the slope at $\lambda = h$ also reveals an interesting trend as ρ increases. The discontinuous change in the value of the slope at $\lambda = h$ is negative for $\rho\sigma^3 < 0.4$, is very nearly zero for 0.4,

and becomes positive for $\rho\sigma^3 = 0.5$ and 0.6, before returning to a negative slope change for $\rho\sigma^3 = 0.7$. Since $\overline{G}(h, h)$ was provided by an approximation, it is questionable whether the observed trend in $\Delta(\partial\overline{G}/\partial\lambda)_{\lambda=h}$, specifically the positive discontinuity in the slope of $\overline{G}$ is reflective of the true behavior in $\overline{G}$. For comparison, Fig. 5 also includes simulation estimates of $\overline{G}$ at $\rho\sigma^3 = 0.6$ and 0.7. Though it is difficult to discern in the figure, close examination of the simulation results at both densities indicates that $\Delta(\partial\overline{G}/\partial\lambda)_{\lambda=h} > 0$. These simulation results along with others not shown confirm the idea that, in light of Eq. 16, the discontinuity is not solely determined by $\left[\overline{G}(h, h) - G(h, \pi, h)\right]/2h$ (which should always be negative) and should still depend upon the integrals over $\partial G/\partial\lambda$ at both $\lambda = h^-$ and $\lambda = h^+$.

As shown in Fig. 8, the I-SPT calculations and simulation results for W at $h = 0.75\sigma$ are again in good agreement at large cavity radii, with no significant differences for $\lambda \geq 3\sigma$. At $\lambda = 3\sigma$, the two differ by less than 1% at all three of the chosen densities. For $\sigma/2 < \lambda \leq \sigma$, however, the differences become greater. At $\rho\sigma^3 = 0.3$, the relative error is minor, remaining below 1%. However, for $\rho\sigma^3 = 0.5$ and 0.6 the relative error exceeds a 2% and 7% overprediction, respectively (in absolute terms, the error is always less than $0.12kT$, but the small value of W amplifies the relative error for these cavity radii). Based on the results presented in Table II, most of the error is probably due to the slight overprediction of $\overline{G}(h, h)$, with some additional error arising from the chosen interpolation scheme. Nevertheless, the simple Laurent series approximation of $\overline{G}$ between $\lambda = \sigma/2$ and h is still quite accurate. For $\lambda > h$, the relative error remains below 1.5% for both $\rho\sigma^3 = 0.3$ and 0.5. For $\rho\sigma^3 = 0.6$, however, the error approaches 7% in the vicinity of $\lambda = h$. Examination of the fitting data indicates that this error arrives via the condition on $W(h, h)$ that was derived from $\overline{F}(\lambda, h)$ (see Eq. 31). For $\lambda = 0.75\sigma$, $\overline{F}(\lambda, h)$ and, hence, $W(h, h)$ becomes increasingly inaccurate as $\rho\sigma^3$ increases[22].

The final case we consider is for $h > \sigma$. Since this region is the largest of all regions, we present I-SPT data for two groups of cavities, one centered at $h = 1.25\sigma$ and another at $h = 3\sigma$. Hence, our discussion includes cavities centered fairly close to the wall where $\rho(z)$ is still oscillating for moderate and high densities and those centered farther from the wall where $\rho(z)$ is effectively uniform except at the highest bulk densities. Figures 9 and 10 contain plots of $\overline{G}(\lambda, h)$ for $h = 1.25\sigma$ and $h = 3\sigma$, respectively. For $h = 1.25\sigma$, $\overline{G}$ exhibits oscillations after $\lambda = \sigma/2$ as it approaches its asymptotic limit that are more

prominent at higher density. These oscillations are much larger than those seen in Fig. 7. For comparison, Fig. 9 includes simulation estimates of $\overline{G}$ at $\rho\sigma^3 = 0.6$ and 0.7. Both simulation traces show oscillatory structure, but while the interpolation is quite accurate at $\rho\sigma^3 = 0.6$, the interpolated $\overline{G}$ is exaggerated at $\rho\sigma^3 = 0.7$. The reasons for this exaggerated behavior are limitations and deficiencies in the interpolation scheme that together give rise to the error. First, as discussed in Section IV A, $\overline{G}(h, h)$ is overpredicted by the approximation in Condition 5 for $\rho\sigma^3 \geq 0.65$. Second, the interpolation scheme fixes the integral of $\overline{G}$ to $\lambda = \sigma$ via Condition 6 instead of the value of $\overline{G}$ itself. Since $\overline{G}(h, h)$ is larger than it should be, $\overline{G}$ is necessarily decreased in some regions such that the condition on $W(\sigma, h)$ is satisfied. This type of error in $\overline{G}$, given the present interpolation scheme and fitting conditions, should be common for high density (as defined by the limitations in our approximation of $\overline{G}(h, h)$) and h in the vicinity of σ. For larger h, the oscillation should become less prominent or nonexistent, since the condition on $W(\sigma, h)$ is further removed from the approximated value of $\overline{G}(h, h)$. Accordingly and among all the interpolation regions, we should expect predictions of $\overline{G}$ and, thereby, W to be least accurate for Regions V, VI, and VII in the vicinity of $\lambda = \sigma$. Consistent with this reasoning, we see in Fig. 10 that the oscillatory structure in $\overline{G}$ is not present for $h = 3\sigma$. As expected, for this value of h, $\overline{G}$ quickly approaches the bulk $G(\lambda)$. For the higher densities, $\overline{G}$ is smaller than $G(\lambda)$ between $\lambda = \sigma/2$ and h, which is another signature of a depletion effect [i.e., $W(\lambda, h) < W(\lambda, h \to \infty)$]. Finally, the discontinuity in the slope at $\lambda = h$ is becoming ever smaller as h increases, being barely perceptible for $h = 3\sigma$. The discontinuity is quite obvious for $h = 1.25\sigma$ at $\rho\sigma^3 = 0.7$, but this discontinuity is likely exaggerated given the previous discussion.

Comparison of $W(\lambda, h)$ predicted by I-SPT to simulation results for $h = 1.25\sigma$ and 3σ yields many conclusions similar to $h = 0.75\sigma$. Figures 11 and 12 contain $W(\lambda, h)$ for the same densities discussed previously, though we have computed the results up to $\lambda = 5\sigma$ for $h = 3\sigma$ so as to examine results for $\lambda > h$. For $h = 1.25$, all three densities exhibit only minor differences between the theoretical and simulation results. The error for $\rho\sigma^3 = 0.3$ does not exceed $0.5kT$, but the error does creep up to nearly $2.2kT$ for $\rho\sigma^3 = 0.5$ and $3kT$ for $\rho\sigma^3 = 0.6$. On a percentage basis, these correspond to less than 1.6% error at $\lambda = 3\sigma$ for all three densities. Thus, as the cavities become large, the I-SPT predictions are still well within the error margins of simulation calculations. Between $\lambda = \sigma/2$ and $\lambda = 1.25\sigma$, however, the percentage error is somewhat larger, which follows from the discussion above

and is consistent with that observed for smaller values of h. For all three densities shown, the error never exceeds 3.1% in this domain of λ where the interpolation is known to be least accurate. It is reassuring to see that the error is smaller than that for $h = 0.75\sigma$, from which we conclude that the simple Laurent series interpolation utilized between $\lambda = \sigma/2$ and h is becoming ever closer to the true form of $\overline{G}$. The improving accuracy is probably also obtained by the increasing accuracy of the approximation for $\overline{G}(h, h)$. Results for $h = 3\sigma$ are much the same case, exhibiting only small differences between the I-SPT predictions and simulation values of W. In fact, on the scale of Fig. 12 the error is not appreciably larger than that for $h = 1.25\sigma$. Examination of numerical results confirms this observation. The results for $\rho\sigma^3 = 0.3$ differ by less than 3% for all values of λ, exceeding 1% only between $\lambda = \sigma/2$ and h. For $\rho\sigma^3 = 0.5$ the error is as much as 2% prior to $\lambda = h$, but remains below 1.6% thereafter. Even in absolute terms the errors for these densities is small, being less than $3.7kT$ in both cases. (This larger error is not of great concern because W is on the order of $650kT$, leading to a small relative error.) At the reduced density 0.6, the error is seemingly larger, becoming as large as $16kT$ at $\lambda = 5\sigma$, but the value of W is about $1100kT$, so the percentage error is only 1.5%. Even for extremely large values of W, I-SPT is proving to be a robust method of computing W, falling within the error margins of simulation in the large cavity limit. The error does, however, give reason for future improvements to I-SPT, perhaps by modifications to the interpolation or fitting conditions. Given the present understanding of I-SPT, the current results strive to be as accurate as possible.

V. COMPARISON OF THE I-SPT $\overline{G}(\lambda, h)$ TO THE SPT $G(\lambda)$: DEPLETION EFFECTS

As follows from Widom's inverse potential distribution theorem[49, 50], or Eq. 29, the local density of a hard-solute sphere or its equivalent cavity at a particular point in the system is related to the reversible work required to insert the cavity at that point. The ratio of the local densities at two locations is therefore determined by the exponential of the difference in the works of insertion at these locations. This difference in works of insertion is nothing more than a potential of mean force defined between these two points, the derivative of which is related to the mean, or effective, force (based on the ensemble average of all the solvent particles) required to keep the solute fixed at a particular location. In the colloidal

literature, this potential of mean force is called a depletion potential, which accounts for the additional (effective) forces that arise between colloidal particles or between particles and various surfaces[23, 24, 31, 59, 60].

A comparison of the relative shapes of $\overline{G}(\lambda, h)$ and bulk $G(\lambda)$ sheds light on the properties of the depletion potential that develops between a cavity (or equivalent solute) and a hard, structureless wall. In a sense, $\overline{G}(\lambda, h)$, as it compares to $G(\lambda)$, is a visual tool that helps in the understanding of depletion effects in hard-particle fluids. As noted above, a depletion potential and its corresponding depletion force exist when the free energy of a particle or other object at some position relative to some inhomogeneity differs from the free energy that particle or object would have in the absence of the inhomogeneity (i.e., either a bulk fluid or a position in the fluid very far from the inhomogeneity). For our system of cavities near a hard wall, a depletion potential exists when the $W(\lambda, h)$ for a cavity differs from $W(\lambda, h \rightarrow \infty)$, where $W(\lambda, h \rightarrow \infty)$ is equal to $W(\lambda)$ for a cavity grown in a bulk HS fluid at the same state point (i.e., bulk density) as the inhomogeneous fluid. As such, the depletion potential, $U_s(\lambda, h)$, is defined as

$$U_s(\lambda, h) = W(\lambda, h) - W(\lambda, h \rightarrow \infty) \tag{40}$$

which using I-SPT and SPT may be expressed as

$$U_s(\lambda, h) = \begin{cases} \int_0^\lambda \rho kT \left[\overline{G}(r, h) - G(r) \right] 4\pi r^2 dr & \lambda \leq h \\ W(|h|, h) - W(|h|, h \rightarrow \infty) + \int_{|h|}^\lambda \rho kT \left[\overline{G}(r, h) 2\pi (r^2 + rh) - G(r) 4\pi r^2 \right] dr & \lambda > h \end{cases} \tag{41}$$

(Note that Eq. 41 provides U_s for all cavities, including those that do not correspond to hard-spheres with positive diameters.) Since U_s is an integral of an appropriate subtraction of $G(\lambda)$ from $\overline{G}(\lambda, h)$, any difference between these two functions may signal a (likely) difference in the corresponding values of W, and so a non-zero value of U_s. We must point out, however, that U_s is not solely determined by the differences in $\overline{G}(\lambda, h)$ and $G(\lambda)$. Each W term in Eq. 40 has different geometric terms in its integrand that are related to the surface area or, equivalently, the differential volume of the cavity. When determining W, $\overline{G}(r, h)$ is multiplied by $4\pi r^2 \rho kT$ for $\lambda \leq h$ and $2\pi(r^2 + rh)\rho kT$ for $\lambda > h$, while $G(r)$ is always multiplied by $4\pi r^2 \rho kT$. Hence, even if $\overline{G}(\lambda, h)$ and $G(\lambda)$ were identical over a given range of cavity radii, U_s would not necessarily be zero for $\lambda > h$ due to possible differences in the (full) volume of the cavity at $h \rightarrow \infty$ and the (nonoverlapping with the $z = 0$ plane)

volume of the cavity at various values of h. In fact, since our analysis already requires $\overline{G}(\lambda, h) = G(\lambda)$ in the limit of $\lambda \to \infty$, we should expect $U_s \neq 0$ at some large $\lambda > h$ by geometric arguments alone.

To better understand how the differences between $\overline{G}(\lambda, h)$ to $G(\lambda)$ may generate the corresponding depletion potential, we plot $\overline{G}(\lambda, h)$ and $W(\lambda, h)$ at $\rho\sigma^3 = 0.6$ for $h = 0$, 0.25σ, 0.5σ and $h \to \infty$ in Figs. 13 and 14, respectively, and Figs. 15 and 16 for $h = 0.75\sigma$, 1.25σ, 3σ and $h \to \infty$. In both sets of figures, $W(\lambda, h)$ is plotted up to a value of λ after which qualitative trends do not change [e.g., $W(\lambda, 0) < W(\lambda, 0.25\sigma) < W(\lambda, 0.5\sigma) < W(\lambda, h \to \infty)$ for Figs. 14] unless otherwise noted. For the following discussion, we focus our analysis on cavities with radii less than $\lambda = 1.25\sigma$. (Note that for these values of λ, the cavity is equivalent to a hard-sphere solute when $h \geq 0.5\sigma$.)

At $h = 0$, the value of $\overline{G}(\lambda, h)$ is larger than $G(\lambda)$ for all λ. But since $h = 0$, the surface area (or differential volume) of the overlapping cavity is much smaller over the entire range of integration than that of the fully spherical cavity. The interplay of these two effects yields $W(\lambda, h = 0) > W(\lambda, h \to \infty)$ for $\lambda < 0.55\sigma$ and $W(\lambda, h = 0) < W(\lambda, h \to \infty)$ at larger radii. Hence, U_s or the depletion potential, is negative for $\lambda > 0.55\sigma$. (While $U_s < 0$ is an "energetically" favorable depletion potential, knowledge of just the sign of U_s alone is insufficient to determine whether the depletion force is attractive or repulsive. Of course, with $U_s \to 0$ as $h \to \infty$, knowing that $U_s < 0$ at a finite value of h implies that an attractive force had to have developed at some value of h, though not necessarily at the given h of interest. By the same argument, $U_s > 0$ requires that a repulsive depletion force arose at some h, which is the case for $\lambda < 0.55\sigma$. Note that for these small cavities, h can become negative before the cavity itself intersects the actual hard wall, located at $h = -\sigma/2$. As these small cavities are moved such that their equivalent hard-sphere comes into contact with the wall, the depletion potential is found to become negative.)

For $h = 0.25\sigma$, the trend is qualitatively identical, with $U_s = 0$ at $\lambda = 0.88\sigma$ and $U_s < 0$ thereafter. The persistence of $W(\lambda, h = 0.25\sigma) > W(\lambda, h \to \infty)$ to a higher value of λ than at $h = 0$ is due to the larger surface area of the cavity for a given λ when $h = 0.25\sigma$ as compared to when $h = 0$. At $h = 0.5\sigma$, the situation is more complex as $W(\lambda, h = 0.5\sigma)$ intersects $W(\lambda, h \to \infty)$ twice. For $\lambda < 0.5\sigma$, $U_s < 0$ owing to the smaller value of $\overline{G}(\lambda, 0.5\sigma)$ as compared to $G(\lambda)$ over this interval. For $0.5\sigma < \lambda < 1.17\sigma$, $W(\lambda, h = 0.5\sigma) > W(\lambda, h \to \infty)$ or $U_s > 0$ due to the much larger value of $\overline{G}$ over this

30

interval. Finally, for $\lambda > 1.17\sigma$, $W\left(\lambda, h = 0.5\sigma\right)$ again becomes less than $W\left(\lambda, h \to \infty\right)$, or $U_s < 0$. Although $\overline{G}\left(\lambda, 0.5\sigma\right)$ is still consistently larger than $G(\lambda)$ for these radii, the different geometric terms appearing in Eq. 41 lead to the appearance of a negative depletion potential. Overall, we find for $h = 0.5\sigma$ that the depletion potential begins with a negative value at $\lambda = 0$, becomes positive as the radius is increased, only to become negative again as λ is further increased.

In Figs. 15 and 16, we return to cases that show a single intersection of $W\left(\lambda, h\right)$ and $W\left(\lambda, h \to \infty\right)$. At $h = 0.75\sigma$, the two work functions intersect at $\lambda = 0.74\sigma$, below which $W\left(\lambda, h = 0.75\sigma\right) < W\left(\lambda, h \to \infty\right)$. U_s and the depletion potential are, therefore, negative for $\lambda < 0.74\sigma$ at $h = 0.75\sigma$. This is entirely due to $\overline{G}\left(\lambda, 0.75\sigma\right)$ being smaller than $G\left(\lambda\right)$ over most of this interval. Thereafter, the surface area/differential volume term is dominant and overcomes the (positive) difference between $\overline{G}$ and G. For $h = 1.25\sigma$, the trend is reversed in that $W\left(\lambda, h = 1.25\sigma\right) > W\left(\lambda, h \to \infty\right)$ up to their intersection point at $\lambda = 0.85\sigma$. This occurs despite the oscillations in $\overline{G}\left(\lambda, 1.25\sigma\right)$ about $G\left(\lambda\right)$. Thus, U_s is positive up to 0.85σ and negative thereafter. For $h = 3\sigma$, there is no discernible difference between $W\left(\lambda, h = 3\sigma\right)$ and $W\left(\lambda, h \to \infty\right)$ up to $\lambda = 0.625\sigma$, which follows from the near equality of $\overline{G}$ and G over the same interval. For $0.625\sigma < \lambda < \sigma$, $W\left(\lambda, h = 3\sigma\right) > W\left(\lambda, h \to \infty\right)$ or $U_s > 0$. Afterwards (not shown in the plot of W), $U_s < 0$ for $\sigma < \lambda < 3\sigma$ and $U_s < 0$ for $\lambda > 3\sigma$. Hence, the depletion potential U_s is, with increasing λ, first negative, then positive, again negative, and again positive.

We can use the results above to assemble the depletion potential profile of a particular λ for successive values of h. For example, if we select $\lambda = 1.25\sigma$ (which corresponds to a hard-sphere of diameter 1.5σ), U_s is negative for $h = 0$, 0.25σ, and 0.5σ, becomes positive for $h = 0.75\sigma$ and 1.25σ, and becomes negative (with a small magnitude) for $h = 3\sigma$. (U_s eventually decays to zero at large enough h.) In turn, as follows from the sign changes in U_s, the depletion force, or $-\partial U_s/\partial h$, also changes sign at various h, exhibiting an attractive region for small and large values of h and a repulsive region at intermediate separations.

This section demonstrates a particular advantage of SPT in describing the depletion potential (or depletion force). Some other methods generate the depletion potential by determining directly the equilibrium arrangement of hard-sphere particles outside of a cavity. While the source of the depletion force is seen via the local arrangement of particles, the physics leading to the depletion potential are somewhat obscured (that is how and why the

arrangement of particles about the cavity changes as the cavity radius is altered). SPT, on the other hand, provides a description of depletion effects that already relies upon those physical and geometric arguments that describe how the average density of hard-sphere particles on the surface of the cavity varies as the cavity center moves away from the wall. As such, SPT more clearly demonstrates that the transitions between attractive and repulsive depletion forces is strongly influenced by the interplay between geometry and the variations of the local density around the cavity.

VI.   CONCLUSIONS

We have presented a fully generalized form of I-SPT that can accurately predict up to moderate bulk densities the reversible work of inserting a cavity of any radius located at any distance from a hard wall. This new version of I-SPT relies upon a number of newly identified conditions, based again on physical and geometric arguments, each of which provides additional insights into the behavior of hard particle fluids near planar surfaces as well as improving the accuracy of earlier versions of I-SPT. Despite its overall success, deviations from simulation results become apparent at bulk densities exceeding $\rho\sigma^3 = 0.7$. Such deviations are consequences of the inherent difficulties in accurately approximating the central I-SPT function $\overline{G}(\lambda, h)$ at the point where the cavity just ceases to intersect the $z = 0$ plane, i..e, $\lambda = h$. Accurate information about this location, or $\overline{G}(h, h)$, is a crucial ingredient in the interpolation scheme needed to represent $\overline{G}(\lambda, h)$ over those cavity sizes and positions where neither exact relations nor thermodynamic arguments can be invoked to describe the surface-averaged local density of hard particles in contact with the cavity surface. While our introduced surface thermodynamic formalism for approximating $\overline{G}(h, h)$ is quite accurate at low to moderate bulk densities, improvements at higher densities are certainly needed and will be the focus of future work in I-SPT.

As noted earlier, the further development of I-SPT was not the only purpose of our current work. With an improved version of I-SPT now available, and in particular a version that can describe all cavities at any distance from the hard wall, we can now employ I-SPT to study the behavior of the line tension of cavities that intersect a planar surface. Recently, the proper boundary thermodynamic relations needed to determine the line tension of hard particle fluids was derived[29], and the generalized version of I-SPT provided here will now

provide the required inputs needed to estimate this important thermodynamic property.

In addition, I-SPT relations were used to predict the depletion potential and depletion force between a hard-sphere solute and a hard wall. As we hoped to have demonstrated, I-SPT is well suited to studying depletion interactions, and provides interesting physical and geometric insights into the origin of depletion effects. Specifically, the interplay between $\overline{G}(\lambda, h)$ and the bulk SPT $G(\lambda)$, which is influenced by the variations in the local density around each cavity, as well as the differences between the differential volumes of the intersecting cavity and the cavity growing far away from the wall, was shown to give rise to the oscillatory nature (attractive and repulsive) of depletion interactions. The accuracy of these predicted depletion potentials, however, needs to be more fully tested. A detailed comparison with depletion interactions determined via molecular simulation is certainly required.

Finally, I-SPT has so far been specifically tailored to describe hard-particle fluids confined by hard, structureless walls. The methods presented here are nevertheless readily extendable to nonplanar geometries, such as curved surfaces or surfaces with given microstructures. For these cases, the resulting equations may not be superficially simple. Yet, I-SPT does offer advantages over other methods when analyzing these more complex surface geometries.

Appendix: Approximation of $\overline{G}(h, h)$ via Boundary Thermodynamics

In this appendix, we present the derivation of our chosen approximation of $\overline{G}(h, h)$ given in Eq. 34. From Widom's potential distribution theorem[49, 50], one may write

$$\frac{\rho(\mathbf{r}_1)}{\rho(\mathbf{r}_2)} = \exp\left[\frac{W_\sigma(\mathbf{r}_2) - W_\sigma(\mathbf{r}_1)}{kT}\right] \tag{42}$$

where $W_\sigma(\mathbf{r})$ is the reversible work of inserting a hard-sphere of diameter σ and $\rho(\mathbf{r})$ is the ensemble-averaged density of the same hard-spheres, both at position $\mathbf{r}$. Equation 42 follows from the uniformity of the chemical potential for an equilibrium system, which accounts for

the local variation of density within an inhomogeneous fluid[49, 50]. Let us now set $\mathbf{r}_1$ as a position on the surface of a cavity of radius λ centered at $z = h$, i.e., $\mathbf{r}_1 = (\lambda, \theta, h)$ using the coordinate system of Fig. 1, and $\mathbf{r}_2$ as a yet unidentified position $\mathbf{r}_{ref}$. Using SPT notation, Eq. 42 becomes

$$G(\lambda, \theta, h) = \frac{\rho(\mathbf{r}_{ref})}{\rho} \exp\left[\frac{W_\sigma(\mathbf{r}_{ref}) - W_\sigma(\lambda, \theta, h)}{kT}\right] \tag{43}$$

After entering Eq. 43 into Eq. 10 with $\lambda = h$, we obtain

$$\overline{G}(h, h) = \frac{\rho(\mathbf{r}_{ref})}{2\rho} \int_0^\pi \exp\left[\frac{W_\sigma(\mathbf{r}_{ref}) - W_\sigma(h, \theta, h)}{kT}\right] \sin\theta d\theta \tag{44}$$

which is nearly identical to Eq. 34. As it stands, Eq. 44 is formally exact.

Since W_σ is not available in general, we require some suitable approximation thereof for use in Eq. 44. Using the analogy between a hard-sphere and a cavity, W_σ may be thought of as the work of growing a cavity of radius σ (a "σ-cule"[1]) centered at the specified position, followed by insertion of the actual hard-sphere at that position. Thus, using boundary thermodynamic concepts that lead to Eq. 26 and are present in every form of SPT, W_σ may be expressed as[37]

$$W(\lambda, \theta, h) = p\Delta V(\lambda, \theta, h) + \sum_i \gamma_i \Delta A_i(\lambda, \theta, h) + \sum_j \tau_j \Delta L_j(\lambda, \theta, h) \tag{45}$$

In Eq. 45, ΔV is the fluid volume that must be emptied of other hard-sphere centers, the ΔA_i are the surfaces that must be created or destroyed, and the ΔL_j are the linear interfaces that must be created or destroyed while growing the cavity. Furthermore, p is the fluid pressure, γ_i is the surface (or boundary) tension of the ith surface, and τ_j is the line tension of the jth line interface. Figure 17(b) illustrates the geometric terms (save for the ΔL_j) for three different hard-spheres/cavities. As noted in the figure, cavities at different positions have different numbers of interfaces.

We may make a simplification to W_σ by ignoring the contribution of linear terms, while still including all the interfacial terms. The line tension terms are, of course, necessary for a proper description of the cavity, but are known to be small contributions compared to the pressure and surface terms[37]. Hence, we drop the linear interface terms and approximate W_σ by

$$W_\sigma(\lambda, \theta, h) \approx p\Delta V(\lambda, \theta, h) + \sum_i \gamma_i \Delta A_i(\lambda, \theta, h)$$

$$\approx p\Delta V(\lambda, \theta, h) + \gamma_\sigma \Delta A_\sigma(\lambda, \theta, h) + \gamma_\lambda \Delta A_\lambda(\lambda, \theta, h) + \gamma_\infty \Delta A_w(\lambda, \theta, h) \tag{46}$$

where the second line separates the sum over $\gamma_i \Delta A_i$ into the possible surface terms. As illustrated in Fig. 17(a), there are three surfaces of importance, the curved surface of radius σ (blue), ΔA_σ, created by the insertion/growth of the σ-cule, the erased curved surface of radius λ (green), ΔA_λ, and the erased portion of wall area (red), ΔA_w. Each area has an associated surface tension that depends on the radius of curvature of the particular surface. The subscript on each γ indicates the radius (and dividing surface[61]) at which that surface tension is evaluated. Figure 17 reveals that ΔA_i is sometimes zero, depending on the position of the σ-cule. For the case of $\lambda = h$ (as shown in Fig. 17), all ΔV and ΔA_i may be computed analytically (see Ref. [45]) and we only need p and γ_i. To obtain those thermodynamic properties, we again use the CS-SPT$_M$ version of SPT[42] since it predicts p and γ_i with high accuracy.

All that remains is the appropriate selection of $\mathbf{r}_{ref}$. Since $\rho G(\lambda, \theta, h)$ is not generally available, we can select a position with $z = 0$, so that the reference hard-sphere is in contact with the confining hard-wall. If this position is far from the cavity of radius λ, the local density at $\mathbf{r}_{ref}$ is equal to p/kT. Finally, with the selection of this reference position and using Eq. 46 for W_σ, we arrive at Eq. 34. The integral may be separated into two parts, one that may be computed analytically and the other that must be computed numerically. For further details, consult Ref. [45].

The limit of $\overline{G}(h, h)$ for $h \rightarrow \infty$ is available from inspection of Eq. 46 with the aid of Fig. 17. As $h \rightarrow \infty$, the work associated with creating a σ-cule cavity that does not intersect the $z = 0$ plane will become identical to $W_\sigma(\mathbf{r}_{ref})$, since the surface of the cavity of radius h is effectively planar, meaning the integrand of Eq. 34 is equal to unity. Furthermore, the domain of θ over which the σ-cule cavity intersects the $z = 0$ plane (where $W_\sigma \neq W_{ref}$) becomes increasingly small, so that the non-overlapping domain is the dominant contribution to $\overline{G}(h, h)$. Therefore, the integral portion of Eq. 34 approaches the value of 2, or $\overline{G}(h, h) \rightarrow p/\rho kT$ for $h \rightarrow \infty$. Estimated limits on derivatives of $\overline{G}$ at $\lambda = h$ are also available from Eqs. 34 and 46 (see Appendix B of Ref. [45]).

The procedure in this appendix that is used to generate $\overline{G}(h, h)$ is similar to that used by Heying and Corti[40] to generate a sixth condition for SPT, though with some important distinctions. In their paper describing SPT$_6$, the term equivalent to $W_\sigma(\mathbf{r})$ was approximated by $\rho kT \Delta V(\mathbf{r})$, which is really a zeroth-order ideal gas approximation. Our approximation of W_σ, which incorporates both pressure and surface tension terms, is a higher-order

approximation that should represent W_σ more accurately than the ideal gas expression.

[1] H. Reiss, H. L. Frisch, and J. L. Lebowitz, J. Chem. Phys. **31**, 369 (1959).

[2] J. L. Lebowitz, E. Helfand, and E. Praestgaard, J. Chem. Phys. **43**, 774 (1965).

[3] R. M. Gibbons, Mol. Phys. **17**, 81 (1969).

[4] M. A. Cotter and D. E. Martire, J. Chem. Phys. **52**, 1902 (1970).

[5] M. A. Cotter and D. E. Martire, J. Chem. Phys. **52**, 1909 (1970).

[6] R. Tenne and E. Bergmann, Phys. Rev. A **17**, 2036 (1978).

[7] A. J. Richard and R. B. Westkaemper, Biopolymers **25**, 2017 (1986).

[8] Y. Rosenfeld, J. Chem. Phys. **89**, 4272 (1988).

[9] M. Irisa, K. Nagayaka, and F. Hirata, Chem. Phys. Lett. **207**, 430 (1993).

[10] F. M. Floris, M. Selmi, A. Tani, and J. Tomasi, J. Chem. Phys. **107**, 6353 (1997).

[11] S. Punnathanam and D. S. Corti, Ind. Eng. Chem. Res. **41**, 1113 (2002).

[12] S. D. Zhang, P. A. Reynolds, and J. S. V. Duijneveldt, Mol. Phys. **100**, 3041 (2002).

[13] S. M. Oversteegen and H. N. W. Lekkerkerker, J. Chem. Phys. **120**, 2470 (2004).

[14] F. H. Stillinger, P. G. Debenedetti, and S. Chatterjee, J. Chem. Phys. **125**, 204504 (2006).

[15] S. Chatterjee, P. G. Debenedetti, and F. H. Stillinger, J. Chem. Phys. **125**, 204505 (2006).

[16] H. S. Ashbaugh and L. R. Pratt, Rev. Mod. Phys. **78**, 159 (2006).

[17] G. Graziano, Chem. Phys. Lett. **432**, 84 (2006).

[18] A. Jain and H. S. Ashbaugh, J. Chem. Phys. **129**, 174505 (2008).

[19] H. S. Ashbaugh, J. Chem. Phys. **130**, 204517 (2009).

[20] D. W. Siderius and D. S. Corti, Phys. Rev. E **71**, 036141 (2005).

[21] D. W. Siderius and D. S. Corti, Phys. Rev. E **71**, 036142 (2005).

[22] D. W. Siderius and D. S. Corti, Phys. Rev. E **75**, 011108 (2007).

[23] S. Asakura and F. Oosawa, J. Chem. Phys. **22**, 1255 (1954).

[24] A. Vrij, Pure Appl. Chem. **48**, 471 (1976).

[25] M. Oettel, Phys. Rev. E **69**, 041404 (2004).

[26] A. R. Herring and J. R. Henderson, Phys. Rev. Lett. **97**, 148302 (2006).

[27] A. R. Herring and J. R. Henderson, Phys. Rev. E **75**, 011402 (2007).

[28] M. Oettel, H. Hansen-Goos, P. Bryk, and R. Roth, Europhys. Lett. **85**, 36003 (2009).

[29] D. W. Siderius and D. S. Corti, J. Phys. Chem. B **113**, 13849 (2009).

[30] P. D. Kaplan, J. L. Rouke, A. G. Yodh, and D. J. Pine, Phys. Rev. Lett. **72**, 582 (1994).

[31] A. D. Dinsmore, A. G. Yodh, and D. J. Pine, Phys. Rev. E **52**, 4045 (1995).

[32] A. D. Dinsmore, A. G. Yodh, and D. J. Pine, Nature **383**, 239 (1996).

[33] R. Dickman, P. Attard, and V. Simonian, J. Chem. Phys. **107**, 205 (1997).

[34] P. Bryk, R. Roth, M. Schoen, and S. Dietrich, Europhys. Lett. **63**, 233 (2003).

[35] L. Harnau, F. Penna, and S. Dietrich, Phys. Rev. E **70**, 021505 (2004).

[36] M. Mastrangeli, S. Abbasi, C. Varel, C. V. Hoof, J. Celis, and K. F. Bohringer, J. Micromech. Microeng. **19**, 083001 (2009).

[37] D. S. Corti and H. Reiss, Mol. Phys. **95**, 269 (1998).

[38] H. Reiss, in *Statistical Mechanics and Statistical Methods in Theory and Application: A Tribute to Elliott W. Montroll*, edited by U. Landman (Plenum, London, 1977), pp. 99–140.

[39] M. J. Mandell and H. Reiss, J. Stat. Phys. **13**, 113 (1975).

[40] M. D. Heying and D. S. Corti, J. Phys. Chem. B **108**, 19756 (2004).

[41] D. W. Siderius and D. S. Corti, Ind. Eng. Chem. Res. **45**, 5489 (2006).

[42] D. W. Siderius and D. S. Corti, J. Chem. Phys. **127**, 144502 (2007).

[43] D. M. Tully-Smith and H. Reiss, J. Chem. Phys. **53**, 4015 (1970).

[44] N. F. Carnahan and K. E. Starling, J. Chem. Phys. **51**, 635 (1969).

[45] D. W. Siderius, Ph.D. thesis, Purdue University (2007).

[46] J. R. Henderson, Physica A **313**, 321 (2002).

[47] V. Botan, F. Pesth, T. Schilling, and M. Oettel, Phys. Rev. E **79**, 061402 (2009).

[48] F. H. Stillinger and M. A. Cotter, J. Chem. Phys. **55**, 3449 (1971).

[49] B. Widom, J. Stat. Phys. **19**, 563 (1978).

[50] B. Widom, J. Phys. Chem. **86**, 869 (1982).

[51] R. C. Tolman, J. Chem. Phys. **17**, 333 (1949).

[52] R. Bragado and G. Navascues, J. Chem. Phys. **68**, 2971 (1979).

[53] G. Navascues and R. Bragado, Phys. Rev. A **28**, 1848 (1983).

[54] R. Bragado and G. Navascues, Phys. Rev. A **29**, 2134 (1984).

[55] D. Henderson, S. Sokolowski, and D. Wasan, J. Stat. Phys. **89**, 233 (1997).

[56] P. Tarazona, Phys. Rev. A **31**, 2672 (1985).

[57] Y. Rosenfeld, Phys. Rev. Lett. **63**, 980 (1989).

[58] E. Kierlik and M. L. Rosinberg, Phys. Rev. A **42**, 3382 (1990).

[59] J. Y. Walz and A. Sharma, J. Colloid Interface Sci. **168**, 485 (1994).

[60] B. Gotzelmann, R. Evans, and S. Dietrich, Phys. Rev. E **57**, 6785 (1998).

[61] M. J. Mandell and H. Reiss, J. Stat. Phys. **13**, 107 (1975).
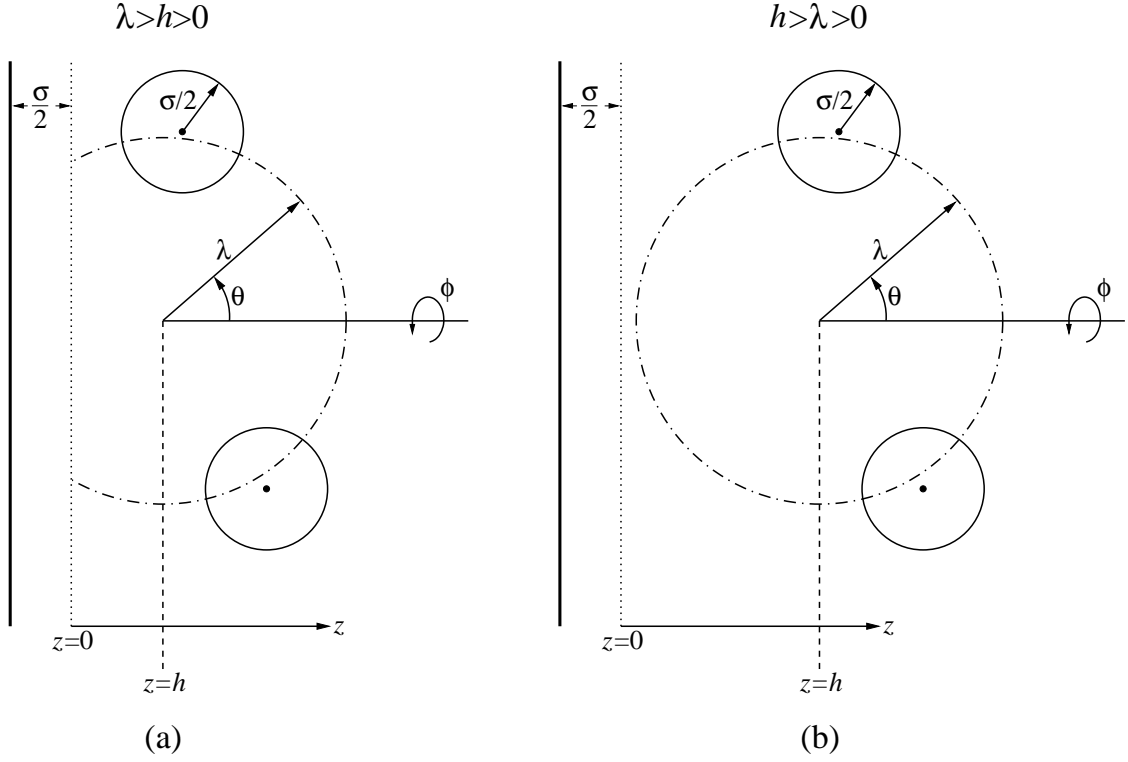
FIG. 1: Coordinate system used to describe cavities near a hard wall. The cavity (represented by the dot-dash line) of radius λ is centered at $z = h$. (a) identifies a cavity centered at $h < 0$, while (b) identifies $h > 0$. In both, the z-axis originates a distance $\sigma/2$ from the hard wall, where σ is the diameter of a HS solvent particle (represented by the solid circles; the centers of the HS solvent particles cannot access the region for which $z < 0$). θ measures the angle originating from a line perpendicular to hard wall and colinear with the cavity center. ϕ describes the rotation around this line. Since the fluid is isotropic in the x- and y-directions, the system is symmetric about ϕ.
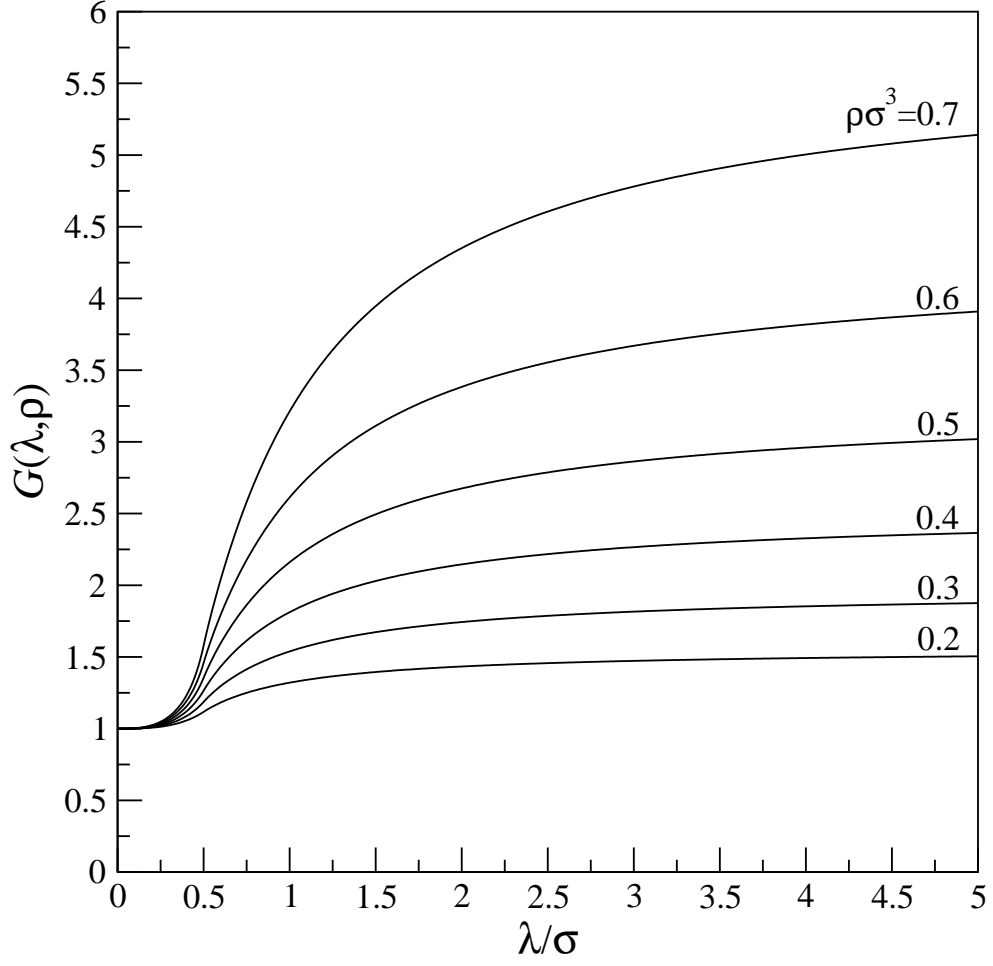
FIG. 2: Plot of $G(\lambda)$ (a cavity in a bulk fluid, or $h \to \infty$) for reduced densities $(\rho\sigma^3)$ between 0.2 and 0.7. The numeric label above each line indicates the reduced density of the plotted line.
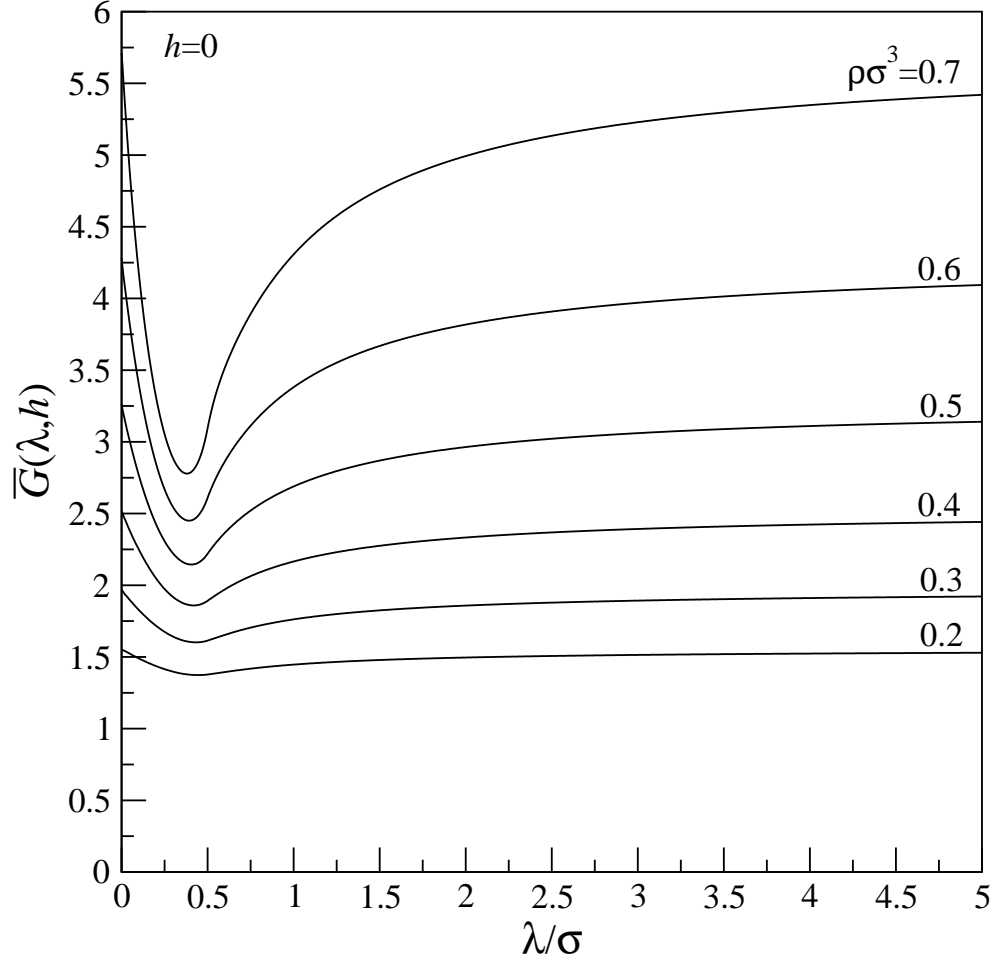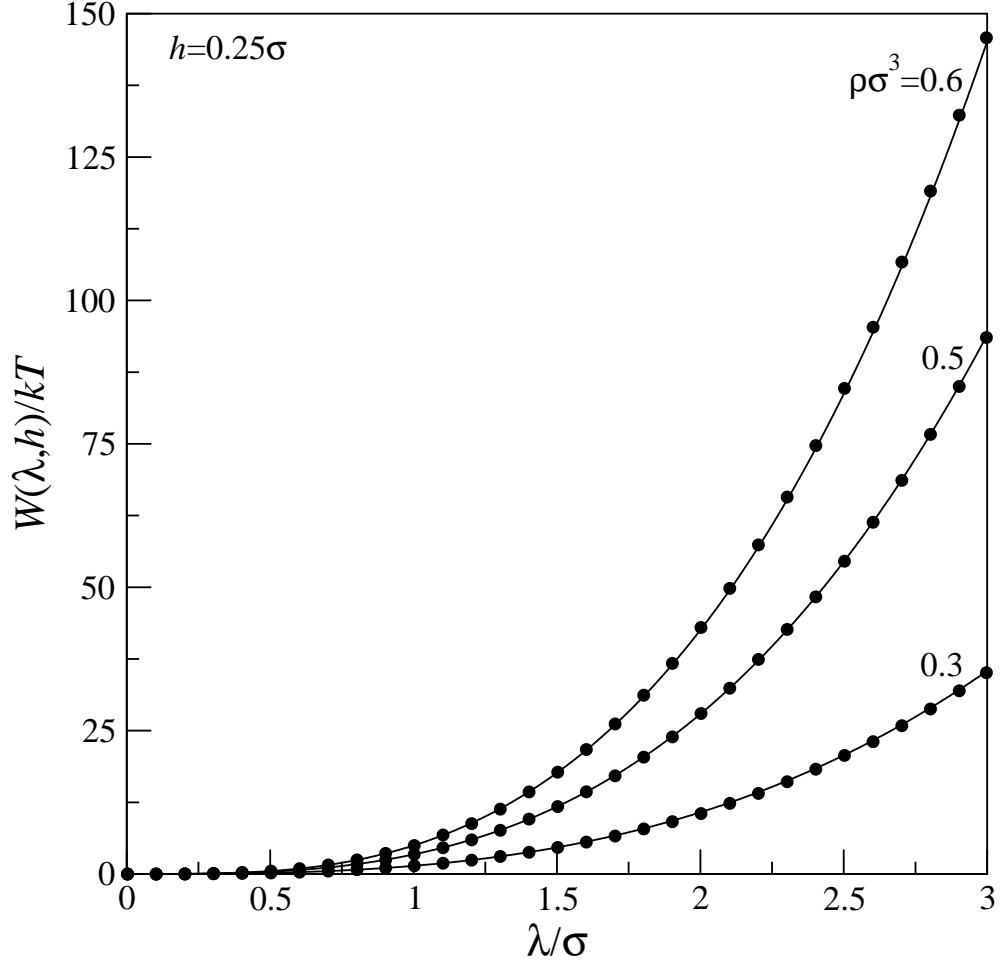
FIG. 3: Plot of $\overline{G}(\lambda, h)$ for $h = 0$ (a hemispherical cavity), for reduced densities $(\rho\sigma^3)$ between 0.2 and 0.7. The numeric label above each line indicates the reduced density of the plotted $\overline{G}(\lambda, h)$. We note in particular that the initial value of $\overline{G}(\lambda, h)$ is $p/\rho kT$, as is the value of $\overline{G}(\lambda, h)$ as $\lambda \to \infty$.
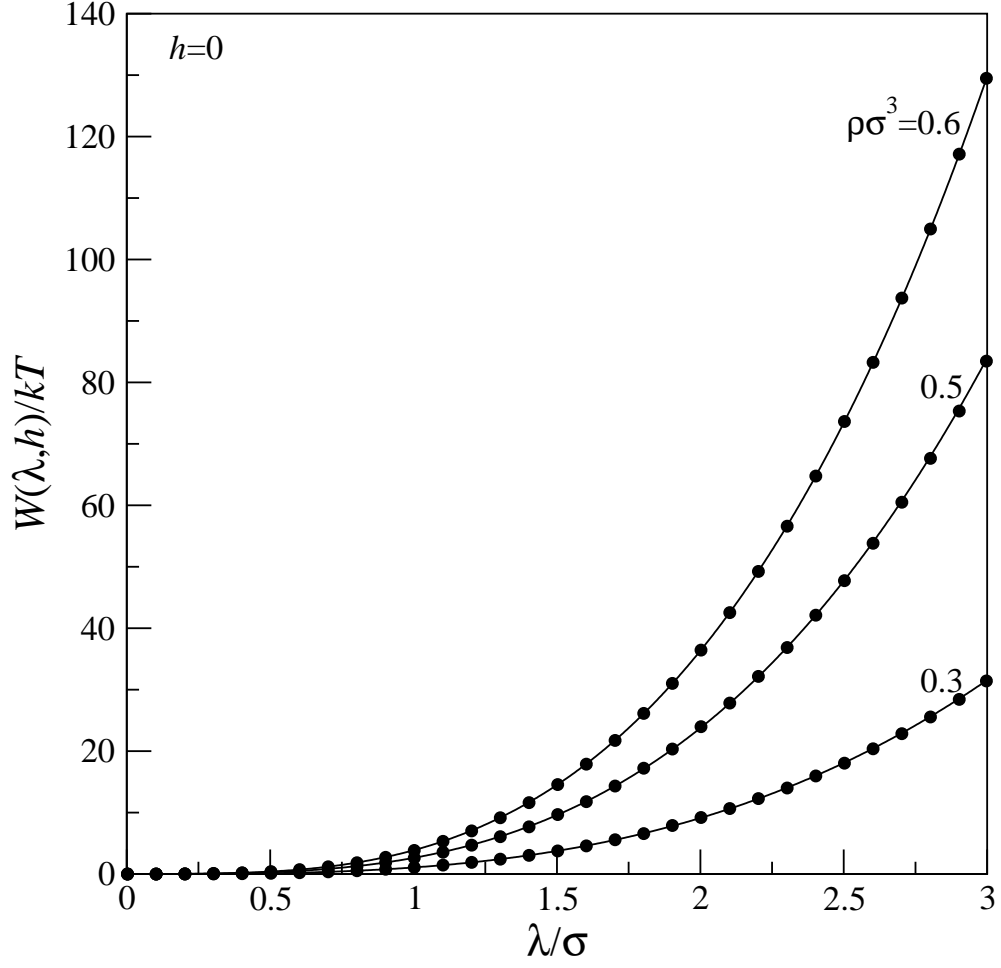
FIG. 4: Work of cavity insertion, $W(\lambda, h)/kT$, for $h = 0$ (a hemispherical cavity), plotted for $\rho\sigma^3 = 0.3$, 0.5, and 0.6. The solid lines are theoretical predictions from I-SPT and the filled circles are calculations from MC simulation. Numeric labels above each data set indicate the reduced density.
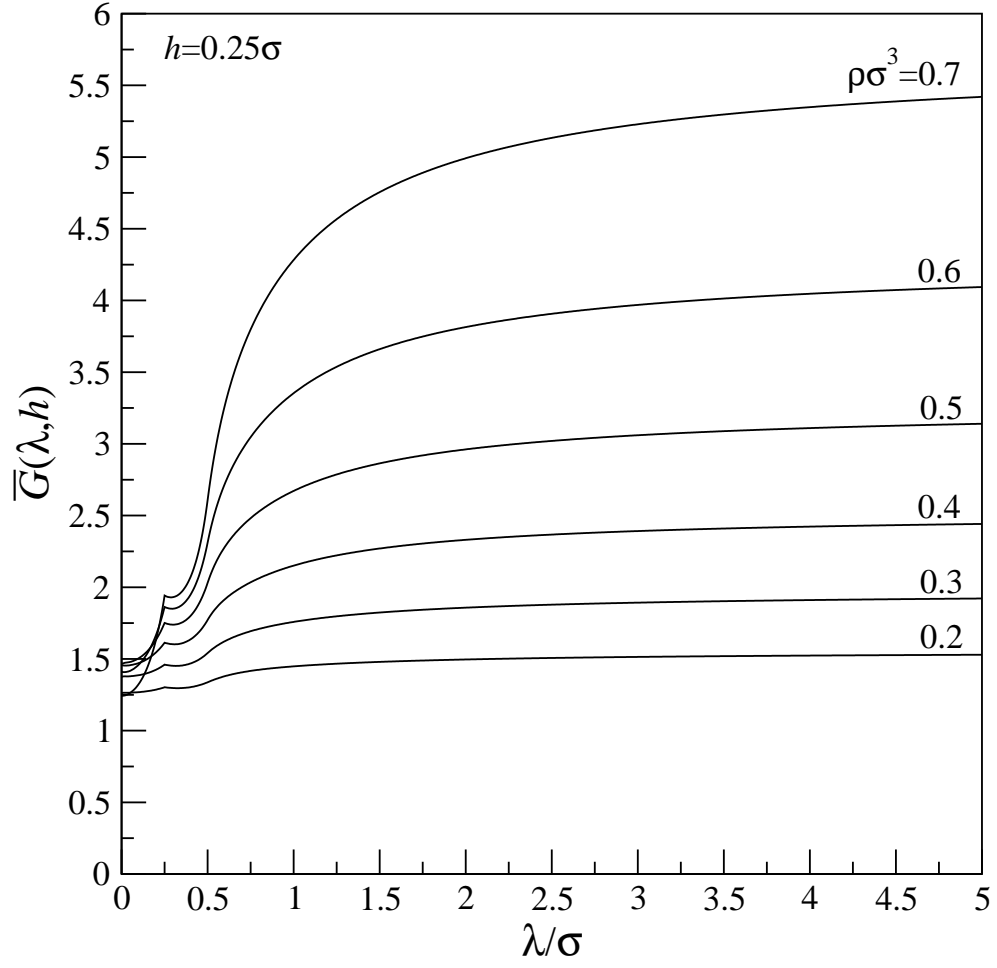
FIG. 5: Plot of $\overline{G}(\lambda, h)$ for $h = 0.25\sigma$, for reduced densities $(\rho\sigma^3)$ between 0.2 and 0.7. The numeric label above each line indicates the reduced density of the plotted line.

FIG. 6: Work of cavity insertion, $W(\lambda, h)/kT$, for $h = 0.25\sigma$, plotted for $\rho\sigma^3 = 0.3$, 0.5, and 0.6. The solid lines are theoretical predictions from I-SPT and the filled circles are calculations from MC simulation.
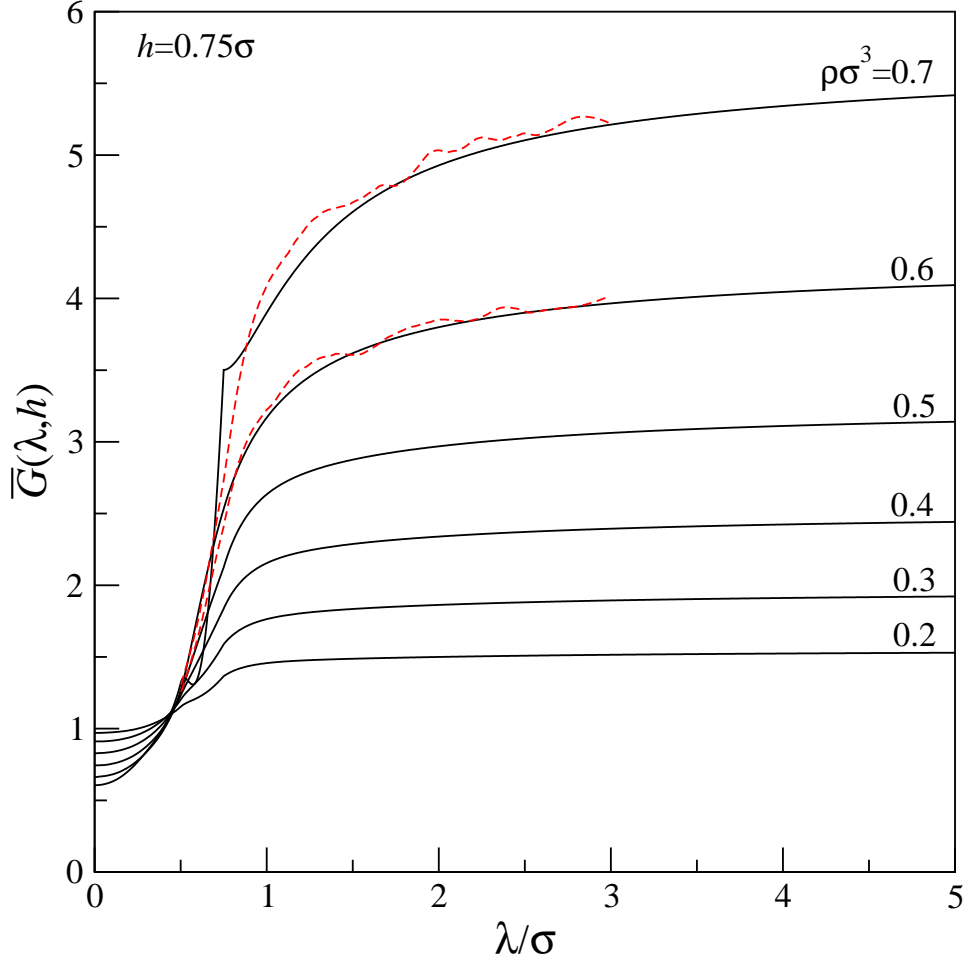
FIG. 7: (Color online) Plot of $\overline{G}(\lambda, h)$ for $h = 0.75\sigma$, for reduced densities $(\rho\sigma^3)$ between 0.2 and 0.7. The numeric label above each line indicates the reduced density of the plotted line. Solid lines are $\overline{G}$ from exact and interpolated calculations. Dashed lines are $\overline{G}$ over $\sigma/2 < \lambda < 3\sigma$ for $\rho\sigma^3 = 0.6$ and 0.7 estimated from simulation measurements of $W(\lambda, h)$ (shown in Fig. 8 for $\rho\sigma^3 = 0.6$).
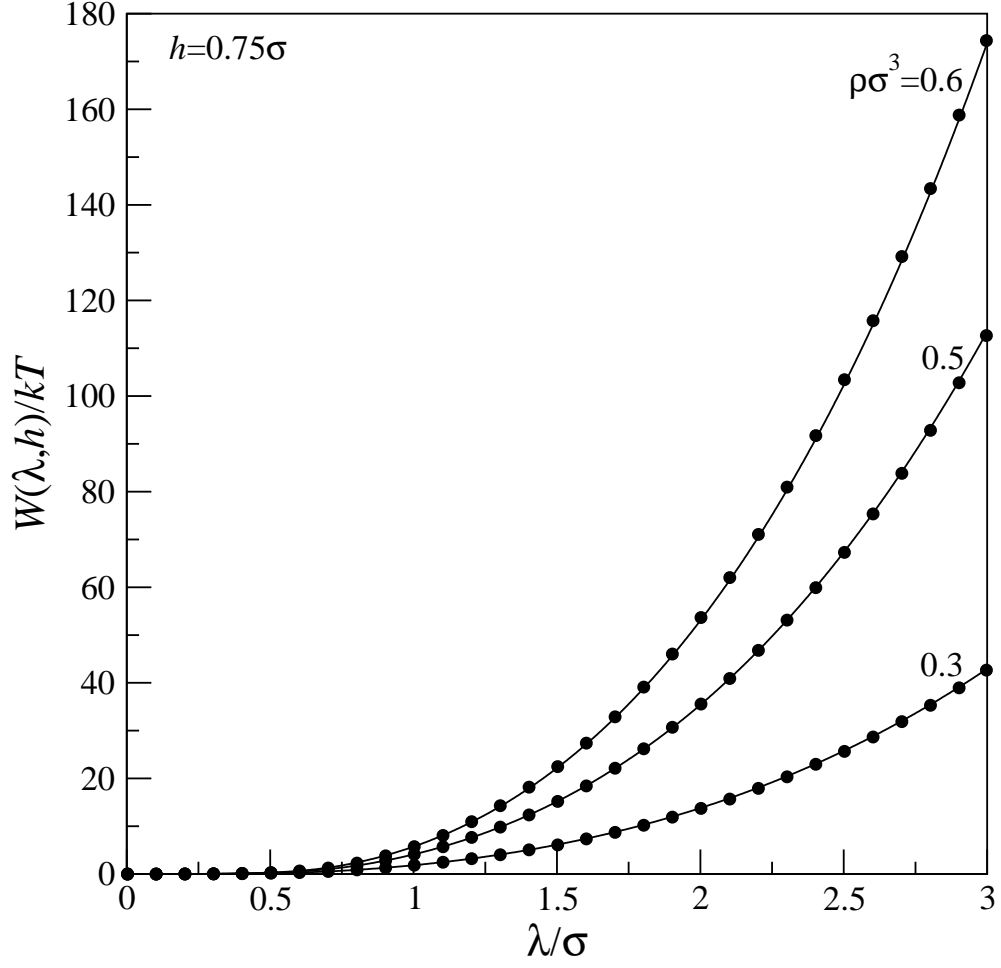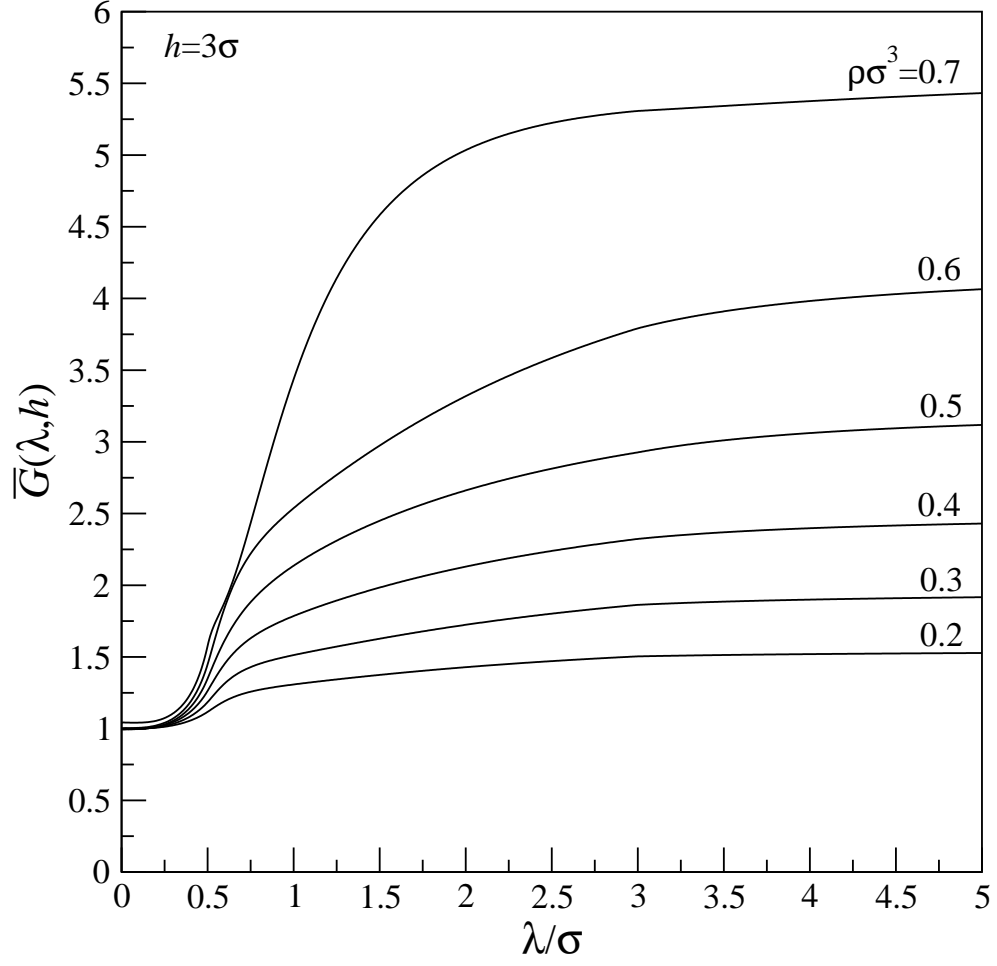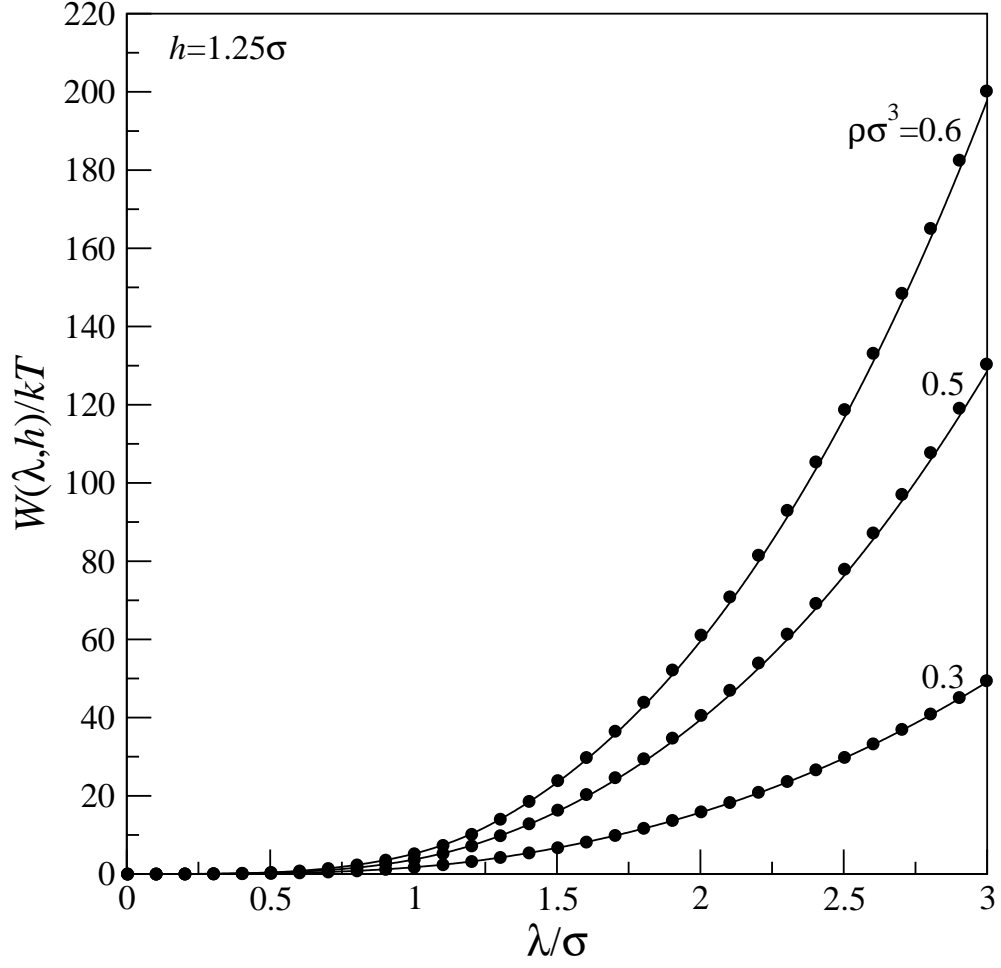
FIG. 8: Work of cavity insertion, $W(\lambda, h)/kT$, for $h = 0.75\sigma$, plotted for $\rho\sigma^3 = 0.3$, 0.5, and 0.6. The solid lines are theoretical predictions from I-SPT and the filled circles are calculations from MC simulation.
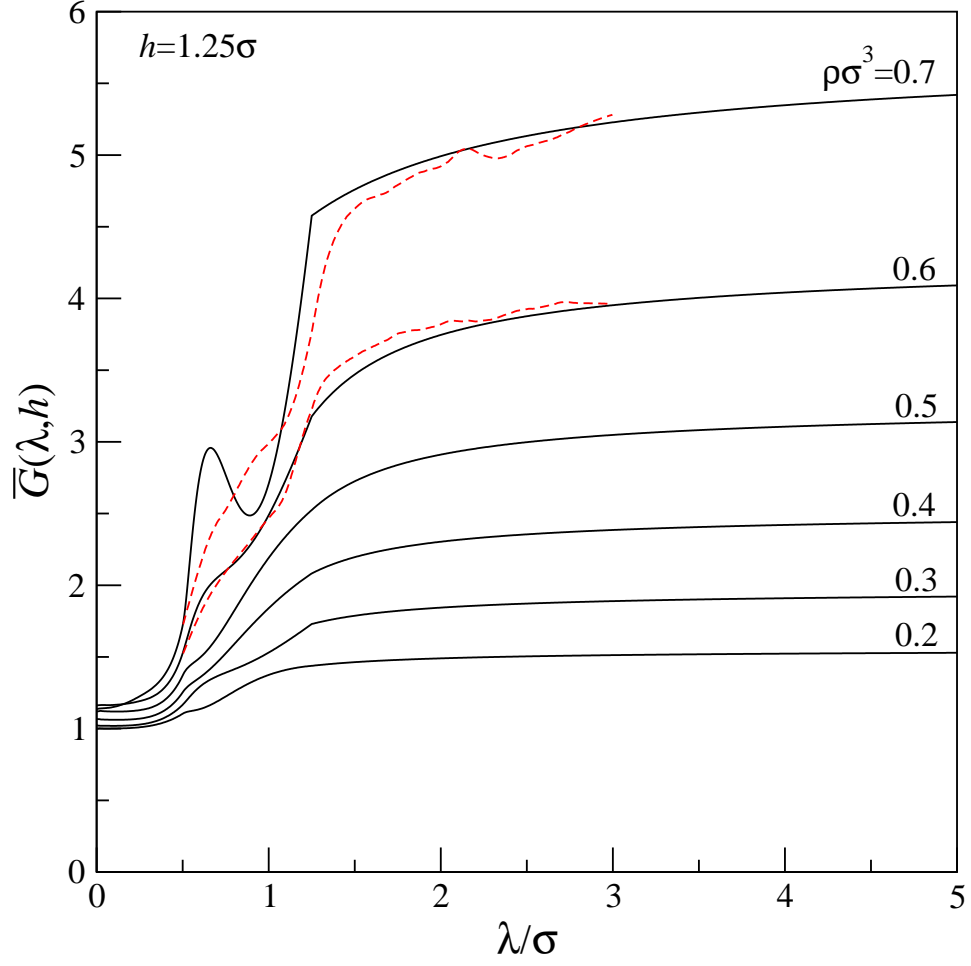
FIG. 9: (Color online) Plot of $\overline{G}(\lambda, h)$ for $h = 1.25\sigma$, for reduced densities $(\rho\sigma^3)$ between 0.2 and 0.7. The numeric label above each line indicates the reduced density of the plotted line. Solid lines are $\overline{G}$ from exact and interpolated calculations. Dashed lines are $\overline{G}$ over $\sigma/2 < \lambda < 3\sigma$ for $\rho\sigma^3 = 0.6$ and 0.7 estimated from simulation measurements of $W(\lambda, h)$ (shown in Fig. 11 for $\rho\sigma^3 = 0.6$).

FIG. 10: Plot of $\overline{G}(\lambda, h)$ for $h = 3\sigma$, for reduced densities $(\rho\sigma^3)$ between 0.2 and 0.7. The numeric label above each line indicates the reduced density of the plotted line.

FIG. 11: Work of cavity insertion, $W(\lambda, h)/kT$, for $h = 1.25\sigma$, plotted for $\rho\sigma^3 = 0.3$, 0.5, and 0.6. The solid lines are theoretical predictions from I-SPT and the filled circles are calculations from MC simulation.
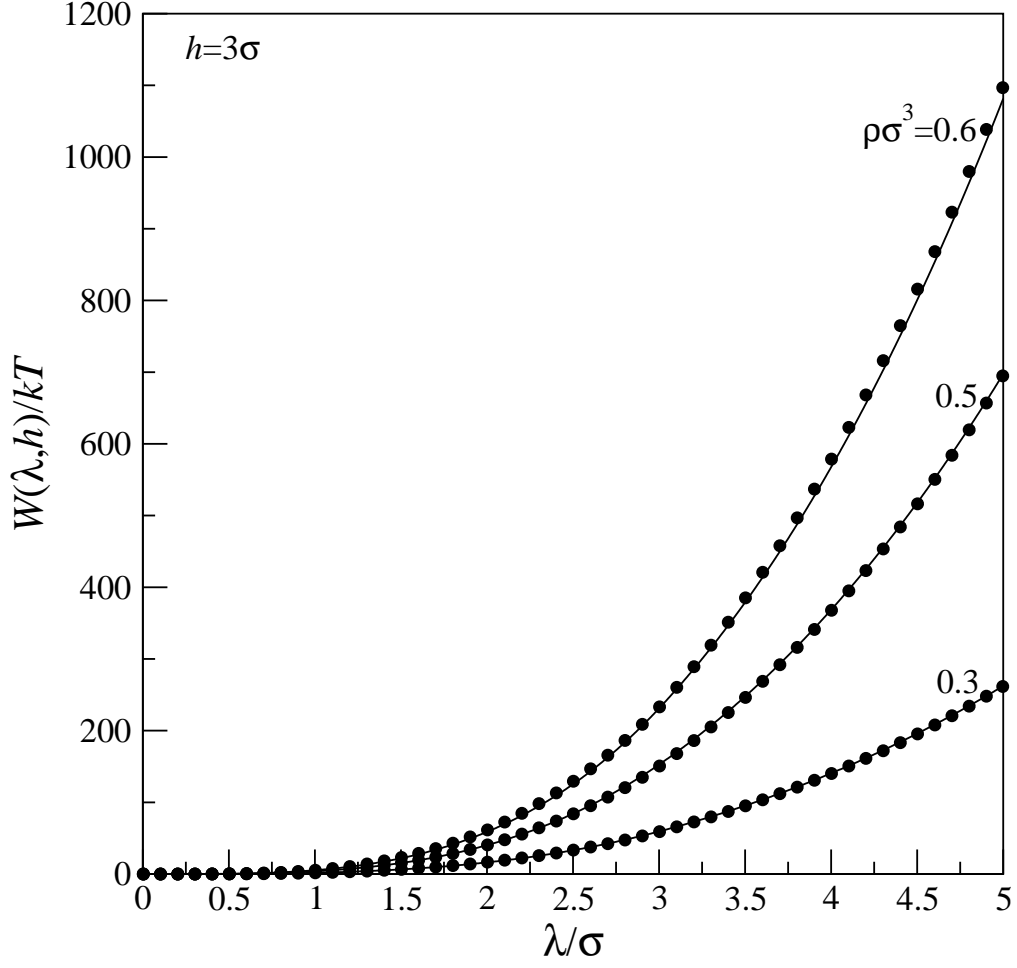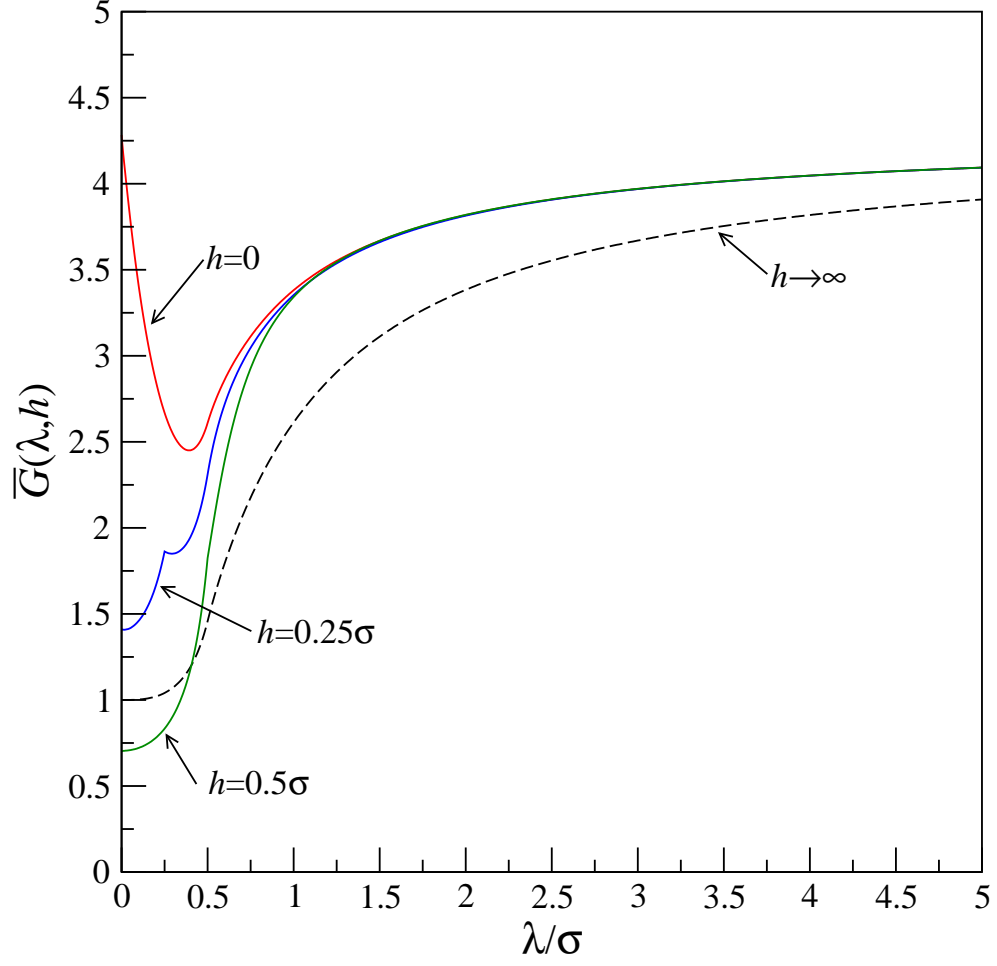
FIG. 12: Work of cavity insertion, $W(\lambda, h)/kT$, for $h = 3\sigma$, plotted for $\rho\sigma^3 = 0.3$, 0.5, and 0.6. The solid lines are theoretical predictions from I-SPT and the filled circles are calculations from MC simulation.

FIG. 13: (Color online) Plot of $\overline{G}(\lambda, h)$ for $h = 0$, 0.25σ, 0.5σ and $h \to \infty$ at $\rho\sigma^3 = 0.6$. Solid lines indicate $\overline{G}(\lambda, h)$, and the value of h for each line is noted. $\overline{G}(\lambda, h \to \infty)$, identical to $G(\lambda)$, is plotted with the dotted line.
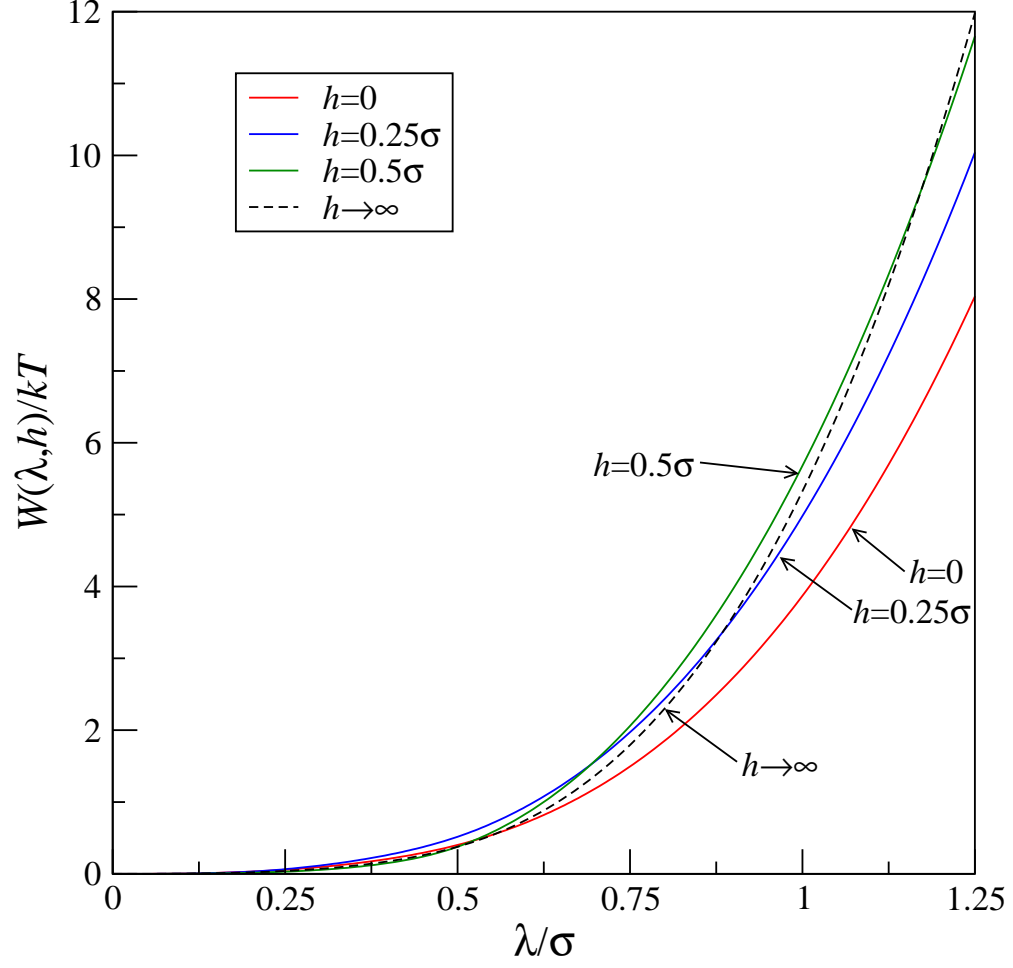
FIG. 14: (Color online) Plot of $W(\lambda, h)$ for $h = 0$, 0.25σ, 0.5σ and $h \to \infty$ at $\rho\sigma^3 = 0.6$. Solid lines indicate $W(\lambda, h)$, and the value of h for each line is noted. $W(\lambda, h \to \infty)$, identical to the bulk SPT $W(\lambda)$, is plotted with the dotted line.
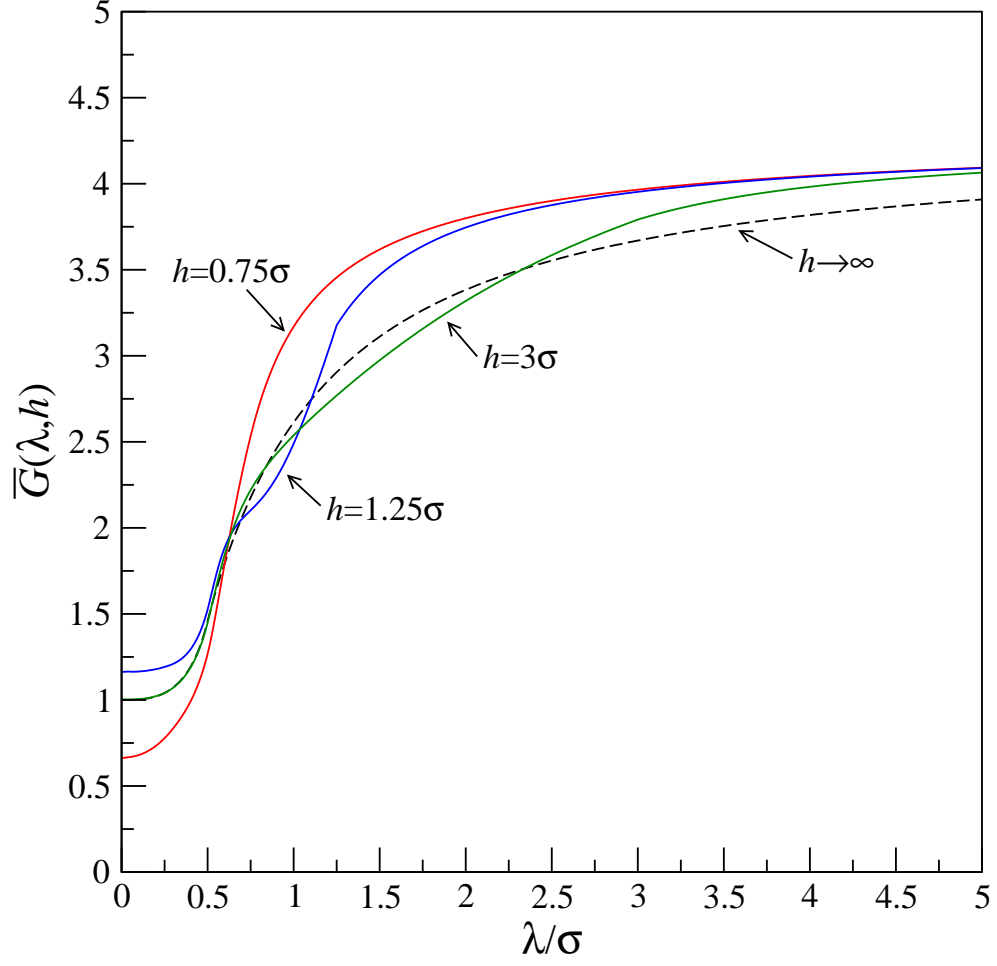
FIG. 15: (Color online) Plot of $\overline{G}(\lambda, h)$ for $h = 0.75\sigma$, 1.25σ, 3σ, and $h \to \infty$ at $\rho\sigma^3 = 0.6$. Solid lines indicate $\overline{G}(\lambda, h)$, and the value of h for each line is noted. $\overline{G}(\lambda, h \to \infty)$, identical to $G(\lambda)$, is plotted with the dotted line.
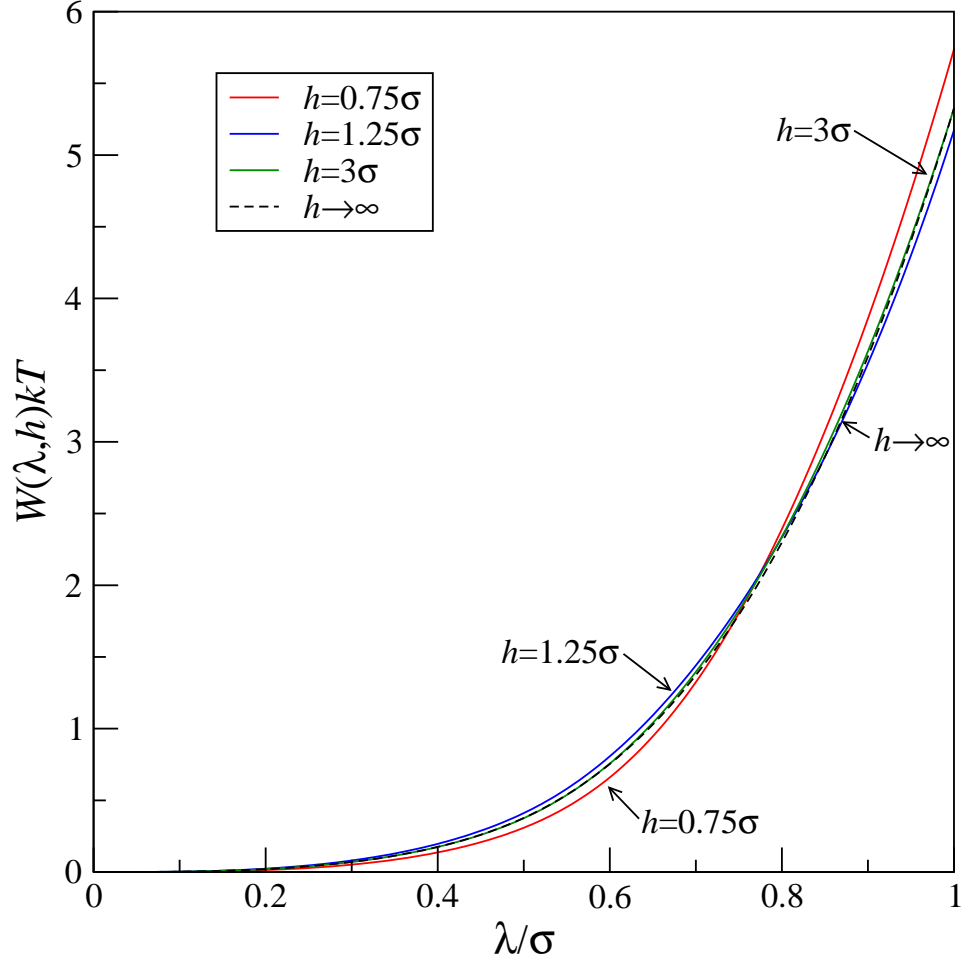
FIG. 16: (Color online) Plot of $W(\lambda, h)$ for $h = 0.75\sigma$, 1.25σ, 3σ, and $h \to \infty$ at $\rho\sigma^3 = 0.6$. Solid lines indicate $W(\lambda, h)$, and the value of h for each line is noted. $W(\lambda, h \to \infty)$, identical to the bulk SPT $W(\lambda)$, is only barely visible on the plot, as it nearly identical to $W(\lambda, h = 3\sigma)$ for the plotted domain.
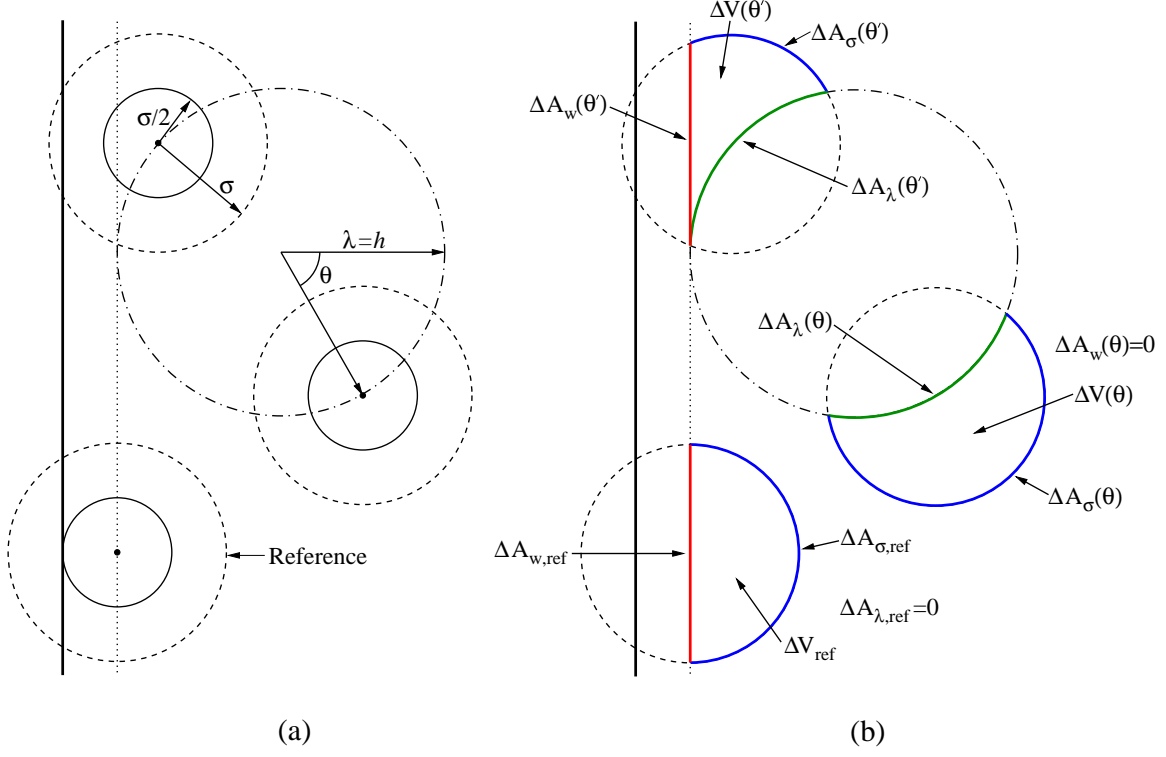
FIG. 17: (Color online) Illustration to aid the explanation of the boundary thermodynamic approximation of W_σ. In (a), a cavity of radius $\lambda = h$ (dot-dash line) is centered at $z = h$ and two hard-sphere particles are placed at distinct positions on the cavity surface and their equivalent σ-cule cavities are shown with dashed lines. A third hard-sphere and its σ-cule are placed at the reference position, which is assumed to be sufficiently far from the cavity such that the cavity of radius λ no longer influences the local fluid. In (b), the hard-sphere particles are removed and the volumes and surfaces associated with the creation of the σ-cule at each position are noted. Insertion of each σ-cule requires the evacuation of a region of volume ΔV and the creation of a surface of area ΔA_σ with radius of curvature σ, noted in blue. σ-cule in contact with the cavity of radius λ require the destruction of some part of the cavity's surface, ΔA_λ which is noted in green. Some σ-cules also destroy part of the wall surface area, ΔA_w, which is noted in red.